SSRG International Journal of Mechanical Engineering
ISSN: 2348-8360/ https://doi.org/10.14445/23488360/IJME-V11I12P105

Volume 11 Issue 12, 47-72, December 2024

Original Article

Formulation and Testing of the Recycled Low-Density Polyethylene Montmorillonite Polymer Composite for Drug Eluting Stents

Ogutu John Bosco[1], Bruno Robert Mose[2], James Mutuku Mutua[2], Christiaan Adika Adenya[3]

[1]*Pan African University, Institute for Basic Sciences Technology and Innovation, Department of Mechanical & Mechatronic Engineering, Nairobi, Kenya.*
[2]*Jomo Kenyatta University of Agriculture and Technology, Department of Mechanical Engineering, Nairobi, Kenya*
[3]*Jomo Kenyatta University of Agriculture and Technology, Department of Marine Engineering and Maritime Operations, Nairobi, Kenya.*

[1]*Corresponding Author : boscoogutu@gmail.com*

Received: 10 October 2024 Revised: 19 November 2024 Accepted: 06 December 2024 Published: 27 December 2024

Abstract *- The increasing global prevalence of Coronary Heart Disease (CAD) has driven the demand for innovative solutions in interventional treatments, with Drug-Eluting Stents (DES) becoming a leading choice. However, the existing stent materials are limited by their biocompatibility and mechanical properties, creating the need for new advancements. This study formulates, tests, and characterizes a polymer composite of recycled low-density polyethylene (rLDPE) and montmorillonite (MMT) for potential application in DES. The research involves material characterization, composite simulation, and optimization using Ansys and Minitab tools, followed by 3D printing of tensile and fatigue test samples to evaluate the composite mechanical properties, alongside morphological analysis using a scanning electron microscope (SEM) to assess material interactions. The Mechanical tests reveal an average tensile strength of 2.46±0.01MPa and fatigue strength of 15.03±0.75MPa, much higher than the primary blood pressure goal in patients with established CAD, which is 0.02MPa. The interaction between rLDPE and MMT effectively produces a homogeneous composite with satisfactory mechanical strength, offering a new material for stent construction. Using rLDPE aligns with environmental sustainability by reducing plastic waste and offering a cost-effective alternative to virgin polymers, making DES more accessible while promoting a circular economy. Montmorillonite acts as an excellent reinforcing agent and drug excipient when incorporated into polymer matrices, improving the mechanical strength, flexibility, and drug release control by enhancing the barrier properties of the composite. The study underscores the potential of rLDPE/MMT composites in addressing modern DES technologies' mechanical, environmental, and biocompatibility demands.*

Keywords *- Drug-eluting stents, Montmorillonite, Morphological property, Polymer composite, 3D printing.*

1. Introduction

Cardiovascular diseases, among them coronary artery disease, continue to be the leading causes of mortality worldwide. The interventional treatment options include balloon angioplasty, stenting, and surgical procedures like bypassing [1]. Drug-Eluting Stents (DES) have, over time, emerged as the preferred choice, providing both structural support to vessels and localized delivery of therapeutic agents to prevent restenosis, a common complication in stent applications[2]. A DES is a vascular prosthesis in a non-surgical treatment called interventional cardiology. It reopens and maintains patent occluded coronary arteries, improving the effectiveness of the drug-based treatment and the concept of controlled Drug Delivery Systems (CDDS) by enhancing delivery to the affected sites. Its structure includes a platform, a coating, and an infused active pharmaceutical agent [3], [4], making it special in its structural material. Its use has steadily risen due to its ease and efficiency in positioning [1]. The development of their materials and the evaluation and analysis of their mechanical properties are consequently significant for better efficacy and enhancement of this treatment technology. A standard material should meet desired properties, including sufficient mechanical strength and ductility, besides biocompatibility requirements [5].

Conventional DES materials of permanent metals, such as stainless steel and cobalt-chromium alloys, provide excellent mechanical strength and biocompatibility, offering the necessary radial support for blood vessels [6]. Cobalt-chromium and platinum-chromium alloys exhibit a high strength-to-weight ratio, allowing for thinner struts in stents, thus improving flexibility and reducing blood flow obstruction

at the implantation sites[7], [8]. This makes them popular in modern DES designs. However, these materials remain in the body indefinitely, leading to chronic inflammation and, in some incidences late-stent thrombosis [9]. Biodegradable metals such as Magnesium and zinc alloys have been on trial. They provide temporary radial vessel support while gradually degrading, consequently minimizing the complications associated with permanency [10]. Magnesium, for example, degrades relatively quickly, leading to premature loss of mechanical integrity needed before fully healing the vessel [11].

Non-biodegradable polymers initially gained use in DES coatings to regulate the release of drugs and provide a stable medium for antiproliferative drugs [12]. They are customizable for different drug-release profiles; however, they have been linked to prolonged inflammatory responses and late stent thrombosis due to their indefinite presence in the vascular environment [13],[14]. Biodegradable polymers, like PLA and PCL, have gained attention as potential alternatives, owing to their ability to gradually degrade and dissolve over time, which reduces t risk of long-term complications [13]. However, the challenge of developing biodegradable materials that maintain structural integrity and control drug release profiles still exists [15]. These materials lead to early stent thrombosis if the drug elution is not adequately controlled [16].

Hydrogels have emerged as promising stent coatings for their hydrophilic nature and potential for smart drug release in response to specific stimuli [17]. They provide a more tailored drug delivery approach adaptable to the patient's physiological environment. However, they are mechanically weak; they cannot independently provide the required structural support, necessitating reinforcement with other materials to serve as viable stent coatings [18].

Graphene and other carbon-based materials have been popular for their high biocompatibility, antimicrobial properties, and strong mechanical strength [19]. They improve the durability and drug-loading efficiency of stents [20]. However, their long-term biocompatibility and behavior in the body, especially their degradation and clearance from the tissues, remain uncertain [21]. More research to understand their potential impacts over extended periods is incomplete.

Polymer nanocomposites are among the current materials under study to enhance DES's mechanical and drug-release properties[22]. They are found to improve drug-loading capacity and allow for controlled drug release. The nanoparticles enhance the material's mechanical stability[23]. Even so, there is a challenge in achieving uniform nanoparticle dispersion. This consequently leads to aggregation, resulting in localized areas of high drug concentration, potentially causing cytotoxic effects and unpredictable release profiles [24]

Generally, from the foregoing review, current materials used in drug-eluting stents and those under study offer unique advantages but also present notable limitations. These challenges consequently prompt other emergency procedures and, at times, lead to fatality. An in-depth analysis of the difficulties indicates the need to incorporate new technologies and materials to ensure better performance [3] [25]. Continuing advancements in material science and engineering are essential for developing safer, more effective DES materials that meet both therapeutic and structural requirements in coronary artery treatment.

An ideal stent should have good mechanical properties, i.e., flexibility and strong radial force, and it should be a table before healing[26]. Therefore, the materials implanted or injected into the human body must be chemically and mechanically stable in the biological environment for long-term use [3]. Additionally, the materials and the processing methods should be cheap to enhance affordability due to the increasing global demand for DESs. In practice, it is almost impossible for all the desired properties to be present in one material. The solution is, therefore, to explore emerging materials such as polymer mixtures or composites [27].

This study formulates, simulates, optimizes, develops, and evaluates a biopolymer composite from recycled low-density polyethylene (rLDPE) and montmorillonite (MMT) for application in drug-eluting stents. These two materials are biocompatible, cheaply available, and mechanically promising. The study's philosophy is that montmorillonite clay with different concentrations would significantly affect the properties of the recycled low-density polyethylene montmorillonite composite due to the nano-dimensional structure and high surface area to volume ratio.

Montmorillonite is a key active constituent of bentonite and a multipurpose clay predominant in medical applications for its unique characteristics of swelling and adsorption. Its high adsorption capacity contributes to increased drug entrapment and sustained release of drugs. It also boosts hydrophobic drugs' dissolution rate and bioavailability[28]. Using recycled low-density polyethylene material intends to contribute to environmental conservation when the world is focused on curbing climate change due to environmental degradation.

This aligns with environmental sustainability by reducing plastic waste and offering a cost-effective alternative to virgin polymers, making DES more accessible while promoting a circular economy. The study also explores the 3D printability of the developed composite and its extension as a method of manufacturing stents. The environmental impact of using rLDPE in stents addresses material sustainability and medical device performance. Incorporating MMT into it results in a composite with enhanced mechanical and morphological properties crucial for stent application.

Life cycle assessments of rLDPE and its composites point to a notable reduction in environmental impact compared to traditional materials. For instance, using rLDPE contributes to waste reduction and a decline in demand for virgin plastic production, contributing to high greenhouse gas emissions and energy consumption [29]. Besides addressing plastic waste management, rLDPE provides a viable alternative for producing composites with enhanced properties [30]. Studies show that adding MMT to rLDPE improves its mechanical strength, thermal stability, and resistance to degradation, making it suitable for medical applications [31],[32]. Previous studies have demonstrated that MMT can improve the tensile strength of rLDPE, one of the essential mechanical properties for the durability and reliability of stents [33],[34]. Additionally, the addition of MMT can alter the crystallinity and morphology of the rLDPE matrix, leading to improved performance characteristics [35]. This further improves stents' efficacy, where mechanical integrity is paramount.

Considering environmental sustainability, using rLDPE and its composites can lead to lower life cycle impacts than traditional materials. Production of conventional stents often uses virgin plastics, which depletes natural resources and generates significant amounts of waste and emissions to the environment [29]. By contrast, utilizing rLDPE reduces the need for new materials and thus promotes a circular economy model in the medical device industry [30].

Integrating recycled LDPE and montmorillonite into stent manufacturing presents a sustainable alternative to traditional materials. The enhanced mechanical properties and reduced environmental impact through recycling position rLDPE/MMT composites as a promising candidate for medical applications.

2. Material and Methods

2.1. Materials

The materials used in this study were recycled Low-Density Polyethylene (rLDPE) pellets, Figure 1(a), of density 917–925 Kg/m3 supplied by Taka Taka Solution Ltd, Kenya, a leading recycling plant in Kenya, and Montmorillonite (MMT), Figure. 1(b), supplied by Swell Well Minechem Pvt. Ltd, Kenya.

(a) **(b)**

Fig. 1 Materials used (a) recycled low-density polyethylene pellets (b) Montmorillonite powder

2.1.1. Material Characterization

Fourier-Transform Infrared Spectroscopy (FTIR)

This analytical technique identifies and quantifies molecular structures based on their infrared (IR) light absorption. Considering the sensitivity of the intended application of the developed composite material, an FTIR spectroscopy was done on the recycled and virgin polymer materials to compare and ascertain the purity, alterations, and microstructural deviations of the recycled LDPE from the Virgin LDPE. It also served to verify the possibility of total recycling of LDPE. This was done using a JASCO FTIR 4700 machine (Japan Spectroscopic Company, Japan). The samples were scanned in the 4000 cm^{-1} to 400 cm^{-1} spectral region, as per ASTM E1252 − 98 (2021), Standard Practice for General Techniques for Obtaining Infrared Spectra for Qualitative Analysis [36] and guided by Jasco 4700 FTIR operation instructions. The attenuated total reflection (ATR) method was used. Two recycled and virgin LDPE samples were evaluated, and results were generated for interpretation.

X-ray Fluorescence (XRF)

This non-destructive analytical technique determines the material chemical composition by measuring the secondary X-rays it emits after exposure to high-energy X-rays. A sample MMT was analyzed to ascertain its elemental composition. This was performed using a portable Bruker S1 TITAN XRF analyzer (Bruker Corporation, Washington USA), according to the ASTM C114-00 Standard Test Methods for Chemical Analysis of Hydraulic Cement [37] and Bruker S1 TITAN XRF analyzer reference manual.

2.2. Methods

2.2.1. Preparation of Polymer Composite

Pellets of rLDPE were dried at 90°C for 2 hours in a UMS-UK laboratory oven (Shanghai Atec Laboratory Equipment Co., Ltd., Shanghai, China) and then cooled to room temperature as per ASTM D6980-17. The cooled rLDPE was then shredded in a 3DEVO-GP20 Plastic Shredding (3devo B.V, Netherlands) to increase the surface area and reduce sizes for a better mixture formation. MMT was dried in the same UMS-UK laboratory oven at 210°C for 1 hour and then cooled to room temperature. The dried MMT material was then passed through available sieves of 75µm and 100 µm to obtain the required particulate sizes. The two materials were weighed on KERN PCB 3500-2 precision balance (KERN & SOHN GmbH, Germany) in portions and mixed in a KLARSTEIN Kitchen mixer (Klarstein of Berlin Brands Group Inc., Germany) for uniform distribution before loading onto the extruder hopper.

2.2.2. Filament Extrusion

Preliminary filament extrusions were done using the SJ35 3D Printing Filament Making Machine (Zhangjiagang, China), varying material compositions, temperature, and extrusion speed. This was to identify the range of extrusion

parameters that gave a continuous material extrude without fume emission, material sputtering, or discoloration of the filament in case of polymer burns besides physical observations of filament diameter, ovality, and consistent running length. The extrusion parameter ranges experimented were 150˚C - 180˚C for extrusion temperature and 18-20 rpm for extruder screw speed.

2.2.3. Design of Polymer Composites

After the preliminary extrusion processes, eight different polymer composites of rLDPE/MMT formulations were developed from varying percentage compositions and particulate sizes of MMT. To create an optimized and reliable composite, a Taguchi mixed-level design of the experiment (DOE) of L8 orthogonal arrays (4^1, 2^1) was used as shown in Table 1; it analyzes experiments where proportions of components are of interest, very commonly used in formulation experiments.

This was executed using Minitab 19 software and simulated using Ansys 2020R1 to predict the mechanical properties of the resulting composites. The two input factors were montmorillonite's percentage weight (wt%) composition and particulate size. The responses expected were the simulated tensile and fatigue strengths.

Table 1. Design of experiment

	Parameters		
Composite ID	**wt% rLDPE**	**wt% MMT**	**Filler size (µm)**
rLDPE/MMT 1	97.5	2.5	75
rLDPE/MMT 2	97.5	2.5	100
rLDPE/MMT 3	95.0	5.0	75
rLDPE/MMT 4	95.0	5.0	100
rLDPE/MMT 5	92.5	7.5	75
rLDPE/MMT 6	92.5	7.5	100
rLDPE/MMT 7	90	10	75
rLDPE/MMT 8	90	10	100

2.2.4. Simulation of Fatigue and Tensile Strengths

The designed composites were simulated using Ansys 2020R1 tools, and the sample models were sketched using solid works, as shown in Figure 3. The Material Designer tool was used to simulate the formulation of the composites, tensile tests using the Explicit Dynamics tool, and fatigue tests using the Transient Structural tool. The tensile test simulations were carried out as per ASTM D638, and the fatigue test simulations were performed according to ISO 1143:2021.

Before the simulations in the tools, the parameters considered for this work were set on Ansys. These included material properties such as Young's modulus, Poisson's ratio, and density; geometric parameters such as sample dimensions, mesh density, element size, and shape; and boundary conditions, loadings, and environmental parameters.

For LDPE, the density was 925Kgm-3, the Young's Modulus was 250MPa, and the Poisson ratio was 0.45; for Montmorillonite, the density was 2500Kgm-3, the Poisson ratio was 0.4. From these, the composite was formulated in predefined ratios.

The drafted 3D models were then uploaded, that is, for tensile the standard dog-bone of dimensions as per ASTM D638 and fatigue as per ISO 1143:2021. Boundary conditions were then set, and loadings were applied. The simulation tests were taken to be at 25ºC.

Assumptions were also made to simplify the model while capturing key mechanical properties relevant to the application, eliminating the complexities of simulating the tensile and fatigue performance.

For the tensile simulation, the composite was assumed to be isotropic and homogeneous and exhibited linear elastic behavior up to its yield point. The test was performed at a constant temperature. That is, there were no thermal effects during the test. On the other hand, for the fatigue test, the composite was assumed to exhibit elastic-perfectly plastic behavior, have no degradation, and be subjected to sinusoidal cyclic loading. The test was not affected by environmental conditions.

2.2.5. Production of 3D Printing Composite Filament

The filament maker SJ35 3D Printing Filament Making Machine (Zhangjiagang, China) was used to obtain the filament. The filament maker comprised three major parts: an extruder, a water bath, and a spooler, as shown in Figure 2. The rLDPE/MMT composite mixture from the kitchen processor was loaded into the single screw extruder. The extruder nozzle diameter was 1.75 mm, compatible with the 3D printing head.

The composite filament extruded from the extruder was cooled through a recirculating water bath and wound onto a spool wheel. The filament spool was loaded on the 3D printing machine to print test samples for tensile and fatigue tests. The extrusion process parameters are as in Table 2.

Table 2. Filament extrusion process parameters

Parameter	**Values**
Barrel Temp (˚C)	165
Die/nozzle Temp (˚C)	170
Screw extrusion speed (rpm)	18
Filament pulling roller speed (mm/s)	250
Filament winding roller speed (mm/s)	150

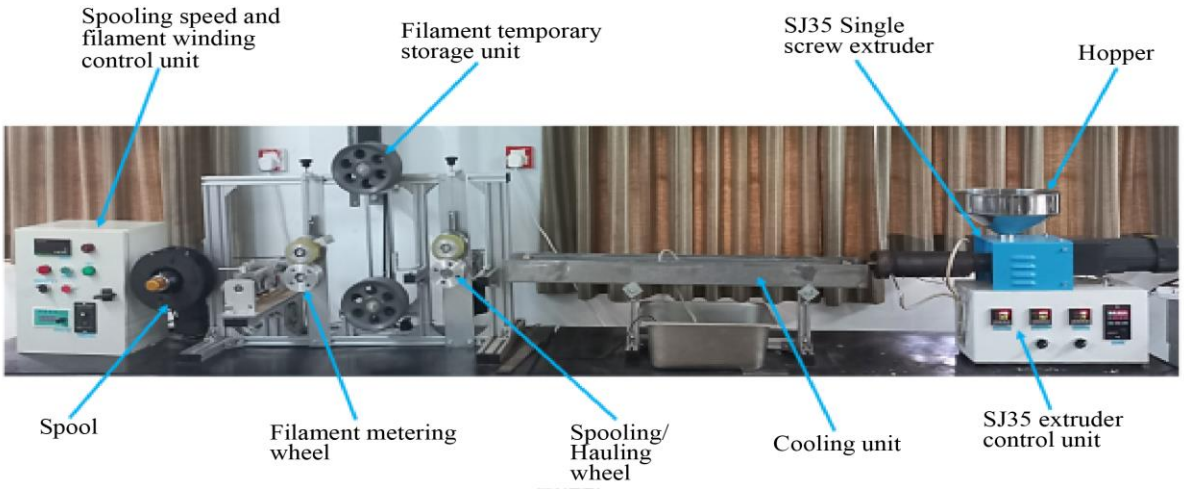

Fig. 2 SJ35 3D Printing Filament Making Machine Assembly [38]

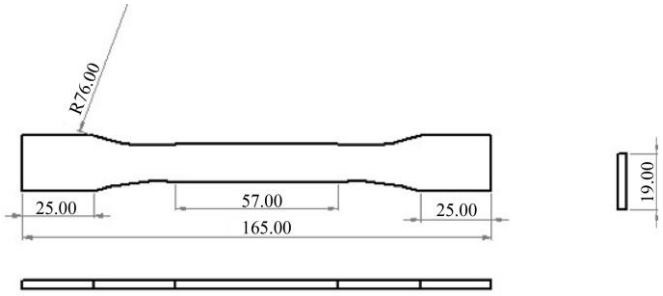

(a)

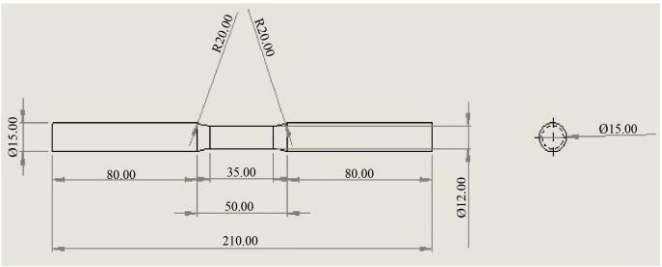

(b)

Fig. 3 Material Test Sample models (a) Tensile Test Sample (b) Fatigue Test Sample

2.2.6. 3D printing of Test Samples

The 3D printing of rLDPE/MMT composites test samples was performed using a Prusa i3 MK3S 3D printer (Czech Republic). The uniaxial testing samples were designed according to ASTM D638 Type I. The typical sketch of the tensile and fatigue samples used in this study is shown in Figure 3(a) and 3(b), respectively.

The sample sketches were converted to STL files, sliced using Prusa slicer software, and forwarded to the 3D printer for printing. The printed test samples, Figure. 4, were printed horizontally, with the filament deposition being longitudinal on a P-Surface 141 to improve part adhesion on the printing surface. The printing parameters during the sample printing are shown in Table 3.

Table 3. Fused filament fabrication printing parameters for samples

Parameters	Values
Printing temperature (˚C)	250
Printing temperature, initial layer (˚C)	250
Build plate temperature, initial layer (˚C)	60
Build plate temperature (˚C)	60
Infill pattern	Rectilinear
Infill (%)	75
Layer height (mm)	0.4
Line width (mm)	0.8
Print speed (mm/s)	50
Initial layer speed (mm/s)	50
Build plate adhesion type	Brim

(a)

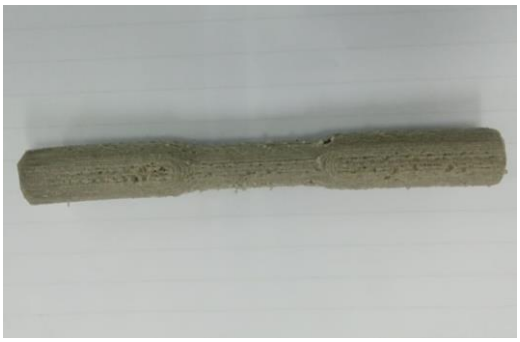

Fig. 4 3D Printed test samples: (a) tensile test sample (b) fatigue test sample

2.3. Characterization of Composite Filament

2.3.1. Scanning Electron Microscope (SEM)

The morphological analysis was done using a JCM-7000NeoScope Benchtop SEM (JEOL USA Inc, Massachusetts, USA) on the extruded filament to observe the MMT powder distribution and the interaction of the compounding materials. The SEM imaging was performed according to ASTM E2809-22 Standard Guide for Using Scanning Electron Microscopy/Energy Dispersive X-Ray Spectroscopy (SEM/EDS) in Forensic Polymer Examinations[39] under an accelerating voltage of 15kV, a Magnification of x200, and a resolution of 100µm.

2.4. Mechanical Tests

2.4.1. Tensile Test

The MMT-reinforced rLDPE blend composite was subjected to tensile tests using a 10kN Shimadzu Autograph AGS-X Series Universal Testing Machine (Shimadzu Corporation, Kyoto, Japan) according to ASTM D638 standard test method for tensile properties of plastics, see Figure 5.

The test samples were 3D-printed tensile test pieces of ASTM D638 Type I, illustrated in Figure 2 (a). They were 165 mm in overall length and width of 19mm with a 50 mm gauge length, a width of 13 mm in the narrow section, and a uniform thickness of 3.2mm.

The equipment had been calibrated, preloading settings were done, and the test sample was clamped and properly aligned, considering the gauge length of 50mm. The tests were performed with one end of the sample fixed and the other pulled gradually at a 5 mm/min speed. It was assumed to be done at a constant room temperature of 25ºC. Five samples were tested, and the average value of the tests was taken as the result. This was used to assess the material's physical strength and any influence of the manufacturing process on it.

Fig. 5 Tensile sample mounted on universal testing machine

2.4.2. Fatigue Test

The fatigue test was performed on ONO's High-Temperature Bending Fatigue Testing Machine Model 7(ONO SOKKI Co. Ltd, Yokohama Japan), see Figure 6. The test samples were prepared by 3D printing. For the sample dimensions, see Figure 3(a), defined by the equipment manufacturer.

The test was performed according to ISO 1143:2021, the rotating bar bending fatigue testing standard. The standard assumed that the material had uniform properties throughout the sample and that the test was conducted in a controlled environment. It also presumed fully reversed loading.

The specimen was then mounted on the rotating bending machine, properly aligned, secured, and centered. A constant bending load of 4kg was applied to create the desired stress level in the gauge section of the specimen. The machine was started and kept a rotation speed of 2165±3rpm, creating a cyclic bending stress with its deflection increasing as it grew weaker. This was run to failure, and the results were recorded. All other samples were done similarly.

Fig. 6 Fatigue sample mounted on ONO's High-Temperature Bending Fatigue Testing Machine Model 7

3. Results and Discussions

3.1. Material Analysis

3.1.1. X-ray fluorescence (XRF) Analysis

Elemental analysis was done on MMT powder to ascertain the elemental chemical composition. The analysis showed that the MMT used was calcium-based, the composition was within their levels, and no elemental contaminants were noticed. The elemental result obtained is contained in Table 4 and presented in Figure 7.

3.1.2. FTIR Analysis

FTIR spectroscopic analysis gives important information about chemical changes in polymer systems due to other processes. To detect these changes, this technology was used to compare the characteristic bands of the polymer compounds.

Attenuated Total Reflectance Fourier-Transform Infrared spectroscope was used to analyze the rLDPE and vLDPE and to evaluate any compositional difference due to recycling and suitability of rLDPE for use in medical applications. Figure 8 shows that these are simple materials with about five peaks and are found in the mid-spectrum of the wavenumber region (400-4000 cm-1), which is divided into four regions: the single bond region (2500-4000 cm-1), the triple bond region (2000-2500 cm-1), the double bond region (1500-2000 cm-1), and (iv) the fingerprint region (600-1500 cm-1) [40]. Narrow bonds of two peaks of wavenumbers 2911.99 cm-1 to 2912.95 cm-1 and 2847.38 cm-1 to 2847.35 cm-1 are observed in all the spectra in the single bond region depicting a C-H stretching. The peaks at 1739.49 cm-1 to 1744.30 cm-1 indicated C=O stretching vibrations of esters. No triple bonds were observed in the spectra. All spectra show the C-H bending at 1462.74 cm-1. At the fingerprint region, there is an indication of –(CH2)-n rocking at 720.28 cm-1 to 722.21 cm-1. Based on the above analysis, the materials, rLDPE and vLDPE, have the same chemical composition. There is no trace of contamination in the rLDPE; therefore, it can be substituted as virgin material, proving the possibility of 100% LDPE recyclability.

Table 4. XRF Results for the Montmorillonite Powder Elemental Composition

Element	% Composition	Element	% Composition	Element	% Composition
MgO	0.000	Cu	0.008	Sb	0.000
Al_2O_3	16.780	Zn	0.012	Ba	0.102
SiO_2	50.350	As	0.000	La	0.000
P_2O_2	0.109	Se	0.000	Ce	0.000
S	0.839	Rb	0.010	Hf	0.000
Cl	0.231	Sr	0.070	Ta	0.000
K_2O	1.309	Y	0.004	W	0.000
CaO	20.955	Zr	0.021	Pt	0.000
Ti	0.917	Nb	0.004	Au	0.000
V	0.006	Mo	0.000	Hg	0.000
Cr	0.001	Rh	0.000	Tl	0.000
Mn	0.101	Pd	0.000	Pb	0.000
Fe	8.167	Ag	0.000	Bi	0.000
Co	0.000	Cd	0.000	Th	0.000
Ni	0.004	Sn	0.000	U	0.000

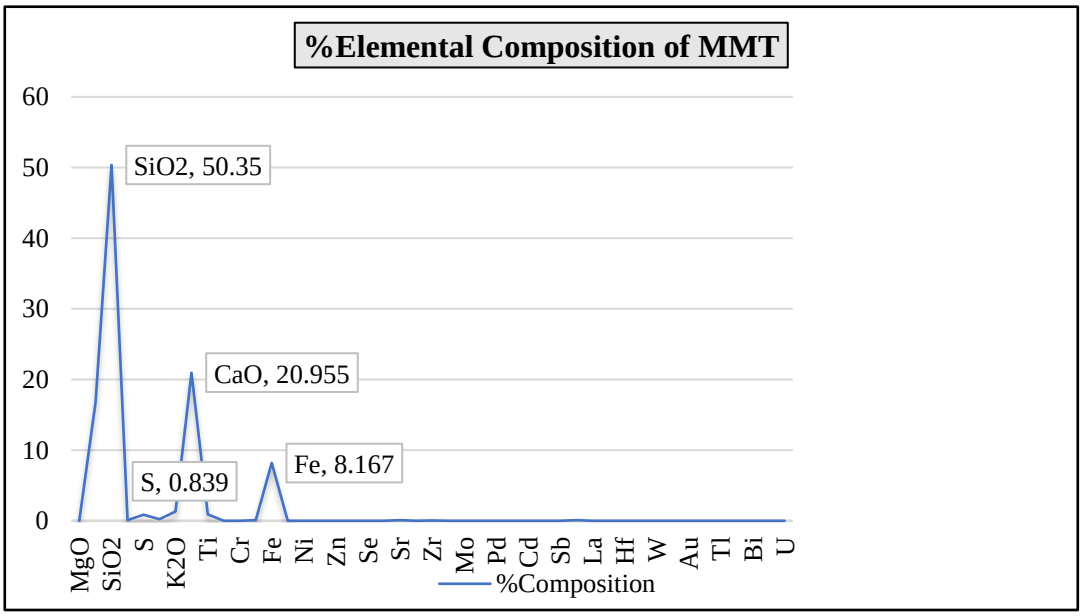

Fig. 7 Graphical presentation of the XRF elemental composition

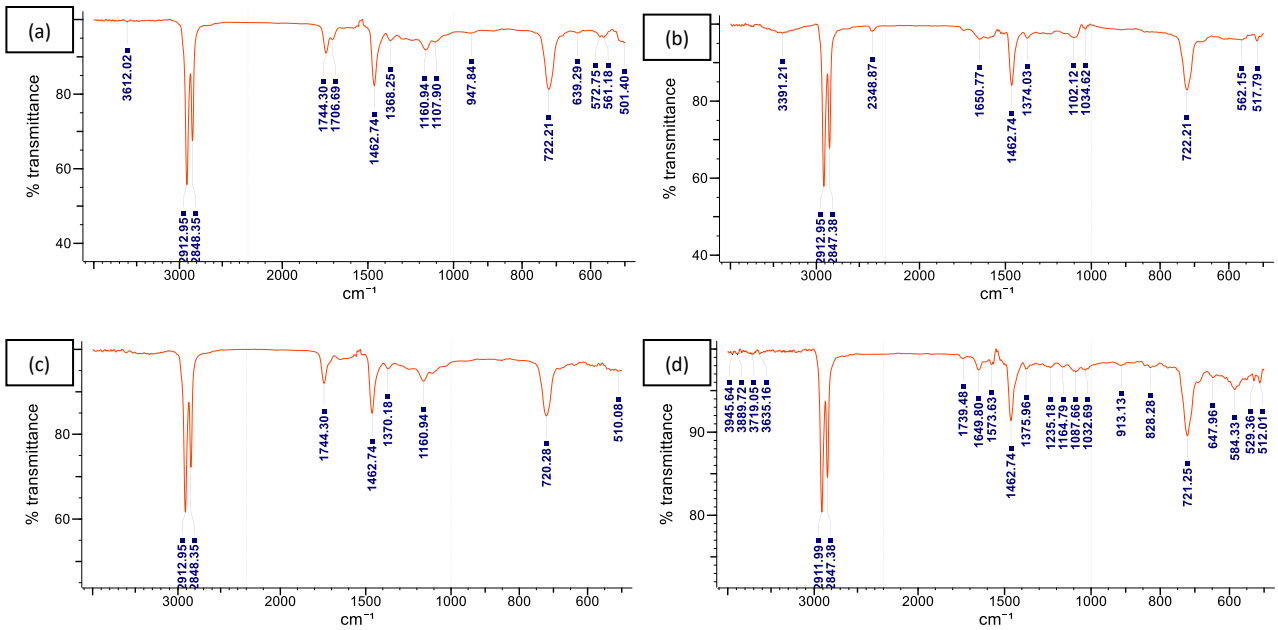

Fig. 8 Fourier-transform infrared spectroscopy results: (a)virgin low-density polyethylene sample 1, (b)virgin low-density polyethylene Sample 2, (c)recycled low-density polyethylene Sample 1, and (d) recycled low-density polyethylene Sample 2

3.2. Preliminary Filament Extrusion Result Analysis

Filament extruded with MMT amount above 20 wt% had inconsistent flow caused by the agglomeration of MMT particles in the screw. The extrusion process parameters were adjusted for MMT above 20 wt%, with no considerable improvement in the filament quality observed. Filament extruded with MMT amount above 10 wt% had a problem with filament collapsing upon cooling. The highest level of MMT content was therefore capped at 10 wt% with 165˚C extrusion temperature and 18rpm for extruder screw speed.

3.3. Simulation of Composite Analysis

The results from the preliminary extrusion informed the formulation of composites designed for simulations. Ansys Workbench was used to run the simulations. Tensile strengths were obtained from Von Mises stresses. Fatigue simulation resulted in Fatigue strength and fatigue safety factors. The simulation results for both tests are captured in Table 5.

The simulation allowed for efficient exploration of parameter space, cost-effective optimization, accurate prediction of complex interactions, and enhanced validation. The results of the simulation were further analyzed as categorically discussed below.

3.3.1. Material Design Simulation

Material design results were obtained using the Ansys Material Designer tool, which incorporates the material percentage composition by weight and particulate sizes of the reinforcing material. The tool gave a randomly distributed filler material within the matrix, depicting a unit physical composite materials interaction structure, Figure 9.

3.3.2. Tensile Test Simulation

Figure 10 below shows the stress distribution for various rLDPE/MMT composites. The color spectrum represents the varying magnitude of the stress experienced in the specimen. The maximum stress in all the specimens occurs at the failure points. The results for minimum and maximum values of Von Mises stress for tensile simulation were obtained. The tensile strength of the composites is observed to increase with increasing weight percentage of MMT and decreasing particle size because smaller particles have a larger surface area for a given particle loading [41].

However, tensile strength eventually decreased once a threshold weight percentage of MMT reached 10%. The simulations evaluated varying design factors and their interactions without conducting every experiment. These results were further subjected to Taguchi DOE to identify optimal combinations of the used parameters that maximize tensile strength.

3.3.3. Fatigue Test Simulation

The simulation results for fatigue strength and safety factor for the rLDPE/MMT composite specimen are shown in Figure 11. From the results, the fatigue strength and safety factor of the composites increases significantly with the increase in weight percentage of MMT and a decrease with the particulate size of MMT. This is because the particulates act as barriers to crack growth planes, hence the crack propagation rate. When the particle size is smaller, the composite's elongation increases, and when the particle size is larger, the composite's elongation decreases because of early fracture caused by particle cracking [42].

Table 5. Summary of the tensile and fatigue simulation results

Run	%Wt MMT	Particulate Size MMT (µm)	Tensile Strength (MPa)	Fatigue Strength (MPa)
1	2.5	75	229.75	57.380
2	2.5	100	235.84	57.373
3	5.0	75	230.54	59.708
4	5.0	100	231.70	59.697
5	7.5	75	260.60	63.483
6	7.5	100	257.50	63.463
7	10	75	286.14	70.012
8	10	100	265.55	69.974

3.4. Taguchi Design Analysis

Taguchi L8 array was employed to obtain a design matrix involving limited experiments covering the whole parametric space. Experiments were performed according to the Taguchi orthogonal array design, and the results obtained were subjected to an optimization process, Table 6. This led to the combination of materials being applied.

Further analysis for optimization was done by employing the probability plots and main effect plots of means, giving an overview of the parametric relation to the responses obtained.

Table 6. Response analysis of the simulation results

Wt.% MMT	Particulate Size MMT (µm)	Tensile Strength (MPa)	Fatigue Strength (MPa)	SNRA1	MEAN1	SNRA2	MEAN2
2.5	75	229.75	57.380	47.2251	229.75	35.1752	57.380
2.5	100	235.84	57.373	47.4523	235.84	35.1742	57.373
5.0	75	230.54	59.708	47.2549	230.54	35.5207	59.708
5.0	100	231.70	59.697	47.2985	231.70	35.5191	59.697
7.5	75	260.60	63.483	48.3195	260.60	36.0531	63.483
7.5	100	257.50	63.463	48.2155	257.50	36.0504	63.463
10.0	75	286.14	70.012	49.1316	286.14	36.9034	70.012
10.0	100	265.55	69.974	48.4829	265.55	36.8987	69.974

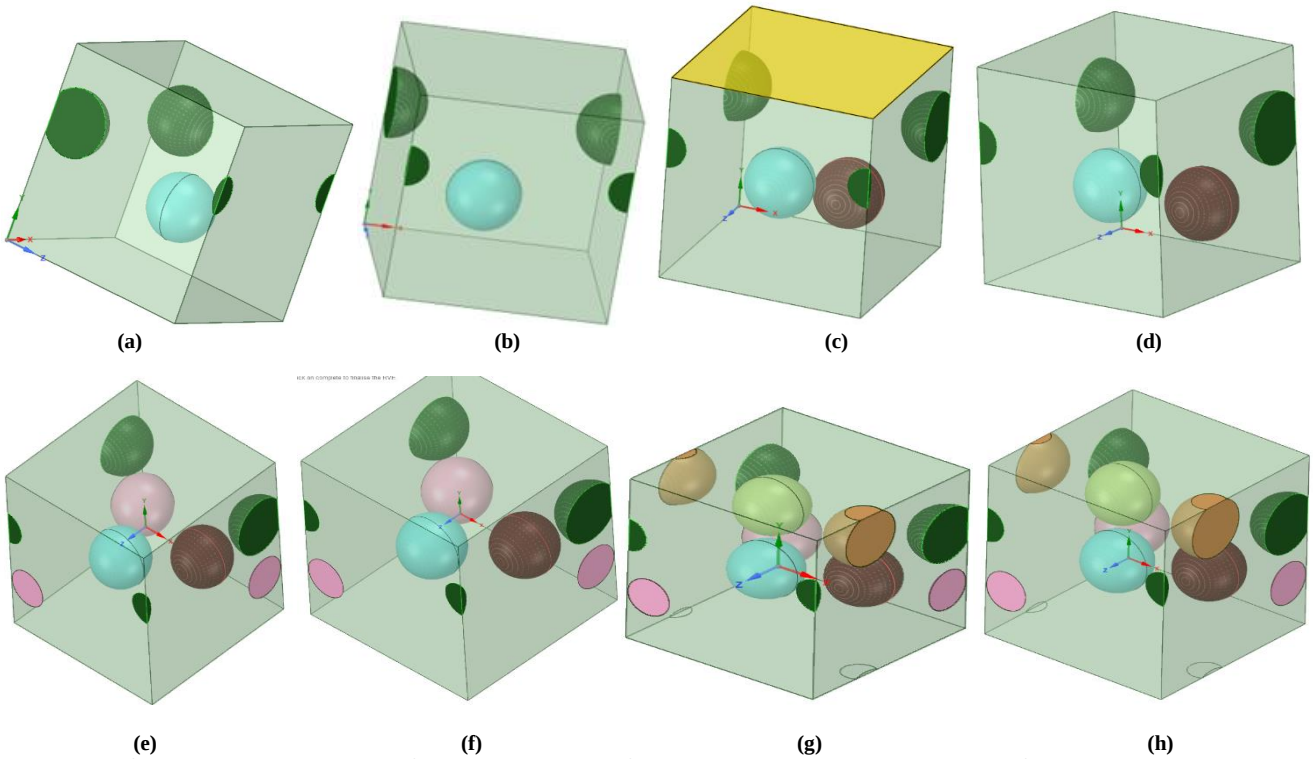

(a) (b) (c) (d) (e) (f) (g) (h)

Fig. 9 Material formulation simulation results for: (a) 2.5%wt MMT of 75µm particulate size, (b) 2.5%wt MMT of 100µm particulate size, (c) 5%wt MMT of 75µm particulate size, (d) 5%wt MMT of 100µm particulate size, (e) 7.5%wt MMT of 75µm particulate size, (f) 7.5%wt MMT of 100µm particulate size, (g) 10%wt MMT of 75µm particulate size, (h) 10%wt MMT of 100µm particulate size.

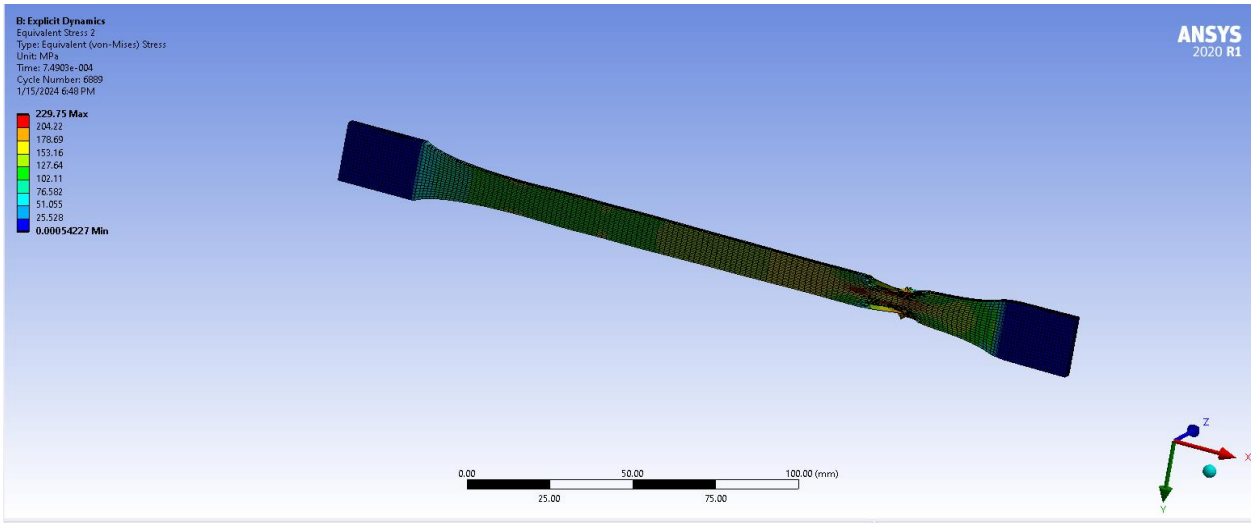
B: Explicit Dynamics
Equivalent Stress 2
Type: Equivalent (von-Mises) Stress
Unit: MPa
Time: 7.4903e-004
Cycle Number: 6889
1/15/2024 6:48 PM
229.75 Max
204.22
178.69
153.16
127.64
102.11
76.582
51.055
25.528
0.00054227 Min
ANSYS
2020 R1
0.00
50.00
100.00 (mm)
25.00
75.00

(a)

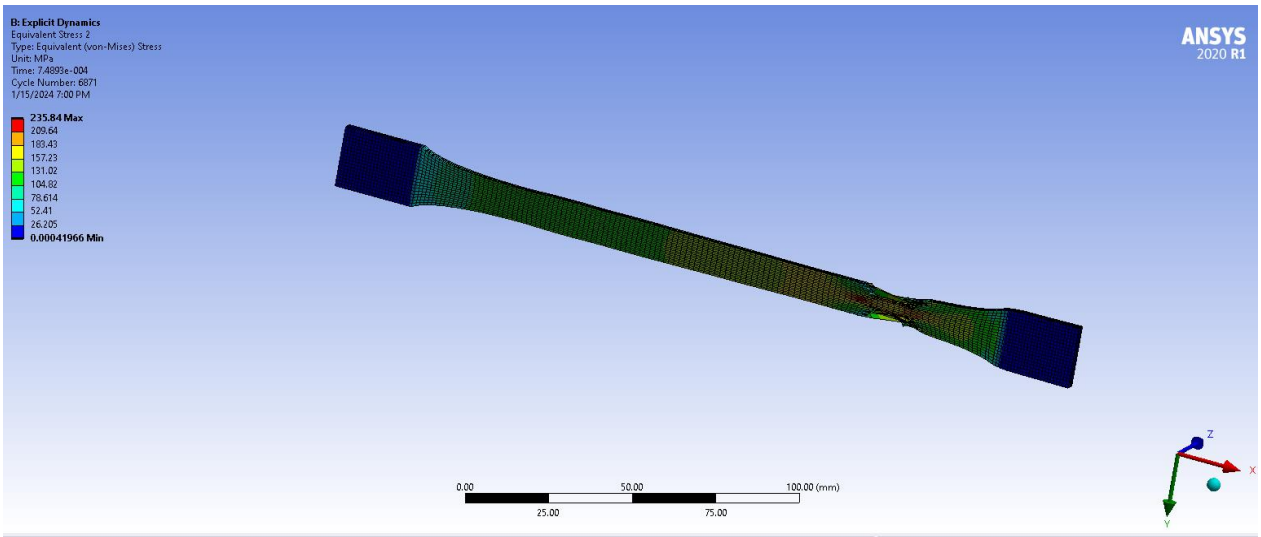
B: Explicit Dynamics
Equivalent Stress 2
Type: Equivalent (von-Mises) Stress
Unit: MPa
Time: 7.4893e-004
Cycle Number: 6871
1/15/2024 7:00 PM
235.84 Max
209.64
183.43
157.23
131.02
104.82
78.614
52.41
26.205
0.00041966 Min
ANSYS
2020 R1
0.00
50.00
100.00 (mm)
25.00
75.00

(b)

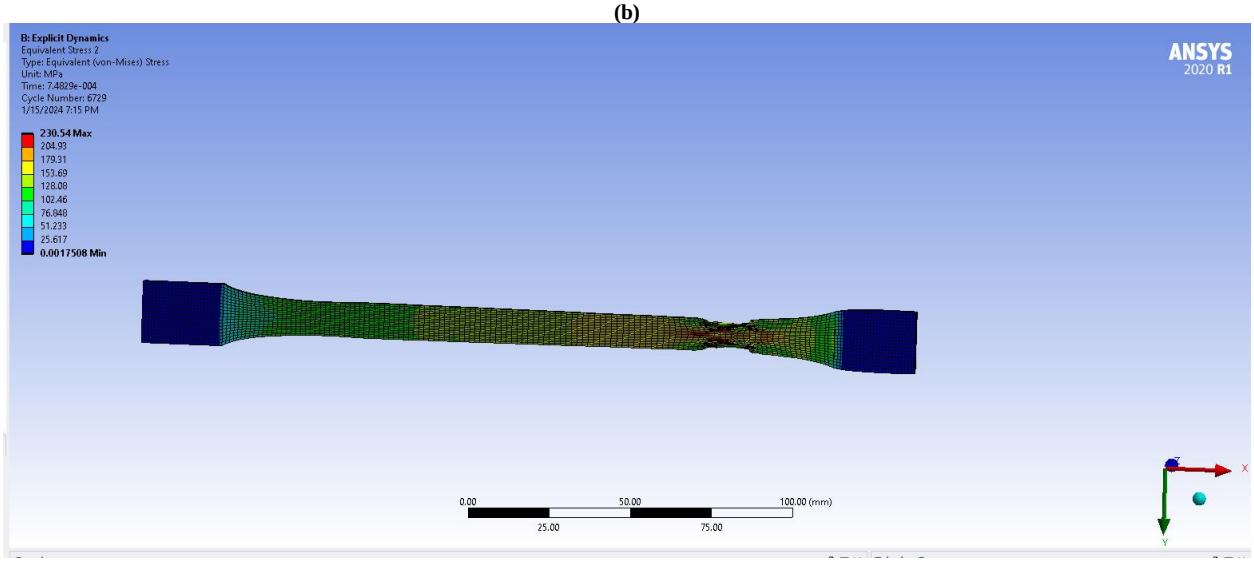
B: Explicit Dynamics
Equivalent Stress 2
Type: Equivalent (von-Mises) Stress
Unit: MPa
Time: 7.4829e-004
Cycle Number: 6729
1/15/2024 7:15 PM
230.54 Max
204.93
179.31
153.69
128.08
102.46
76.848
51.233
25.617
0.0017508 Min
ANSYS
2020 R1
0.00
50.00
100.00 (mm)
25.00
75.00

(c)

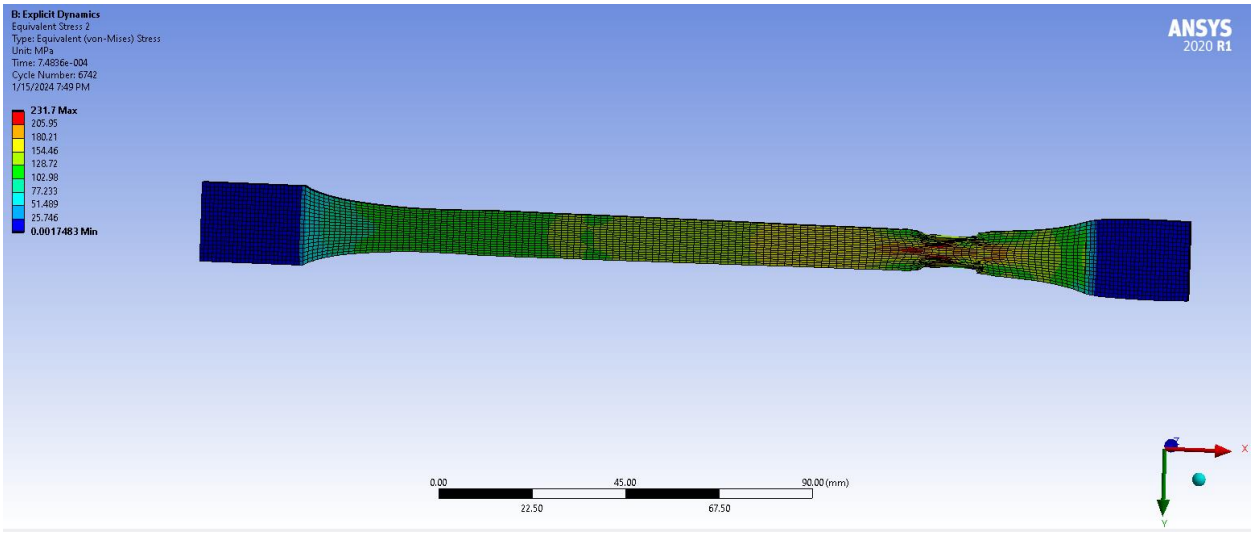
B: Explicit Dynamics
Equivalent Stress 2
Type: Equivalent (von-Mises) Stress
Unit: MPa
Time: 7.4836e-004
Cycle Number: 6742
1/15/2024 7:49 PM
231.7 Max
205.95
180.21
154.46
128.72
102.98
77.233
51.489
25.746
0.0017483 Min
ANSYS
2020 R1
0.00
45.00
90.00 (mm)
22.50
67.50

(d)

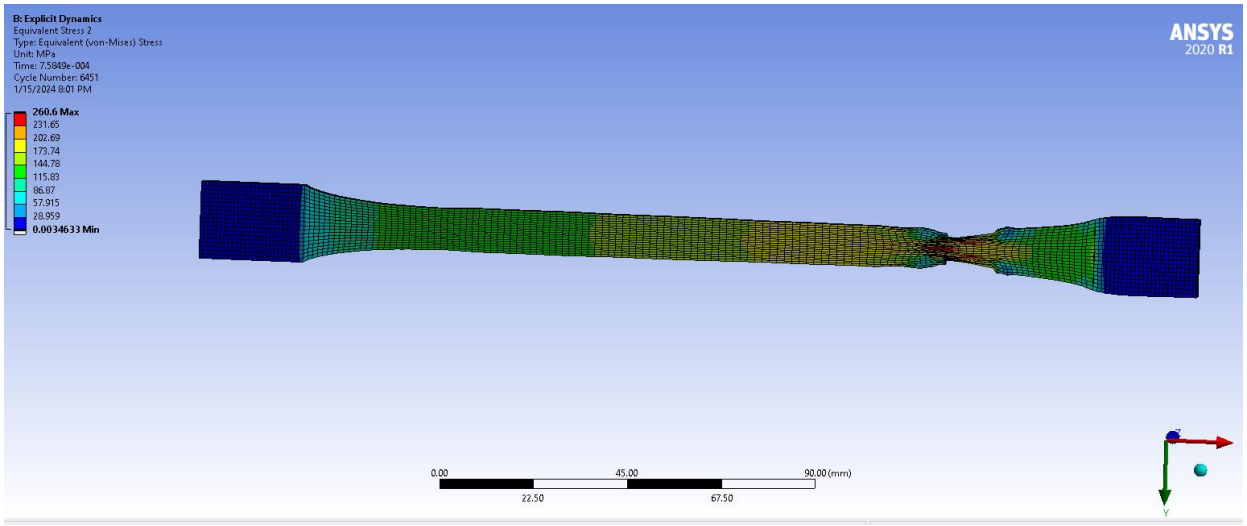
B: Explicit Dynamics
Equivalent Stress 2
Type: Equivalent (von-Mises) Stress
Unit: MPa
Time: 7.5949e-004
Cycle Number: 6451
1/15/2024 8:01 PM
260.6 Max
231.65
202.69
173.74
144.78
115.83
86.87
57.915
28.959
0.0034633 Min
ANSYS
2020 R1
0.00
45.00
90.00 (mm)
22.50
67.50

(e)

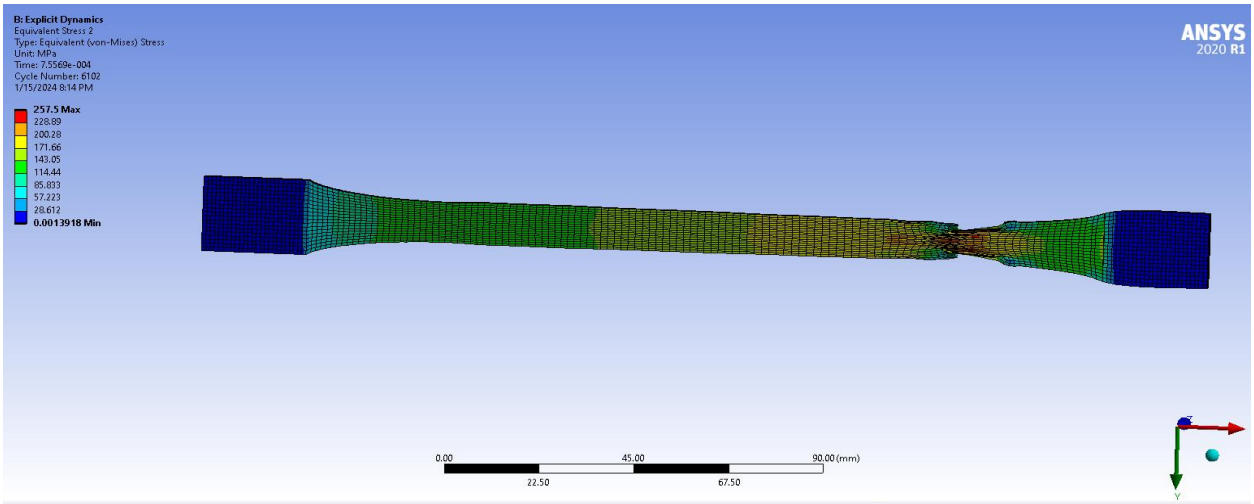
B: Explicit Dynamics
Equivalent Stress 2
Type: Equivalent (von-Mises) Stress
Unit: MPa
Time: 7.5569e-004
Cycle Number: 6102
1/15/2024 8:14 PM
257.5 Max
228.89
200.28
171.66
143.05
114.44
85.833
57.223
28.612
0.0013918 Min
ANSYS
2020 R1
0.00
45.00
90.00 (mm)
22.50
67.50

(f)

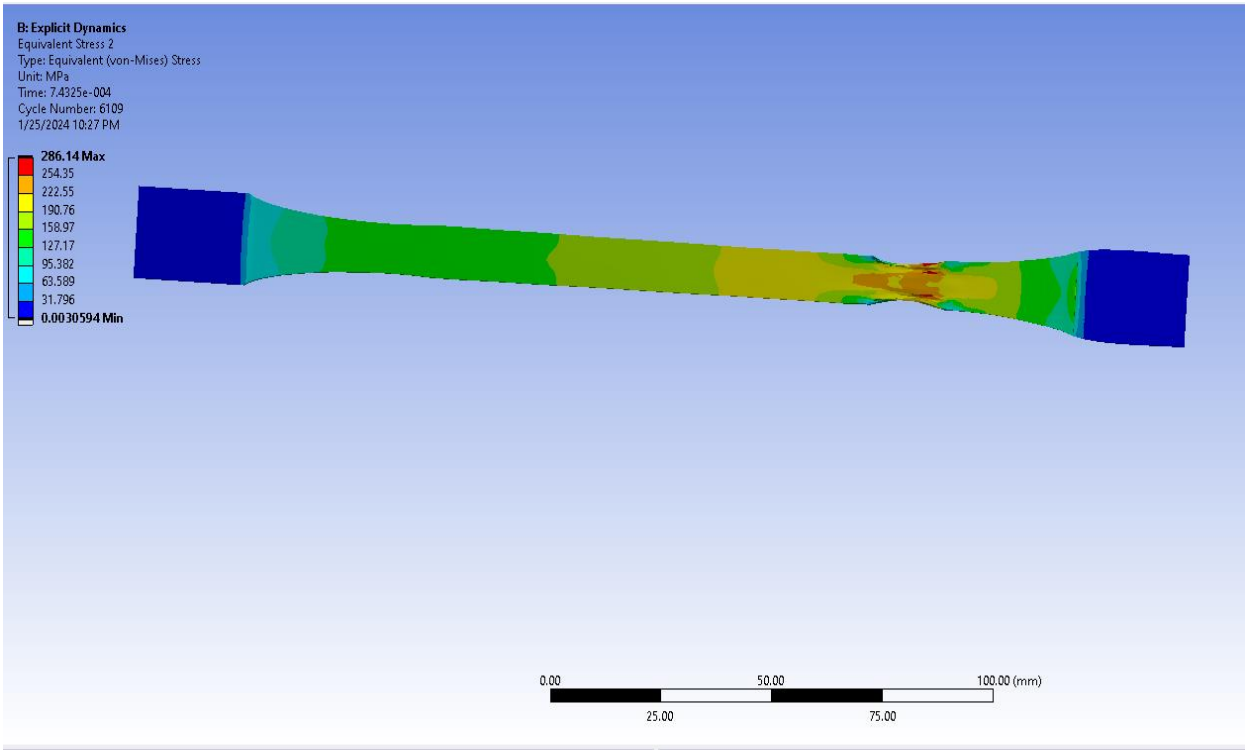

(g)

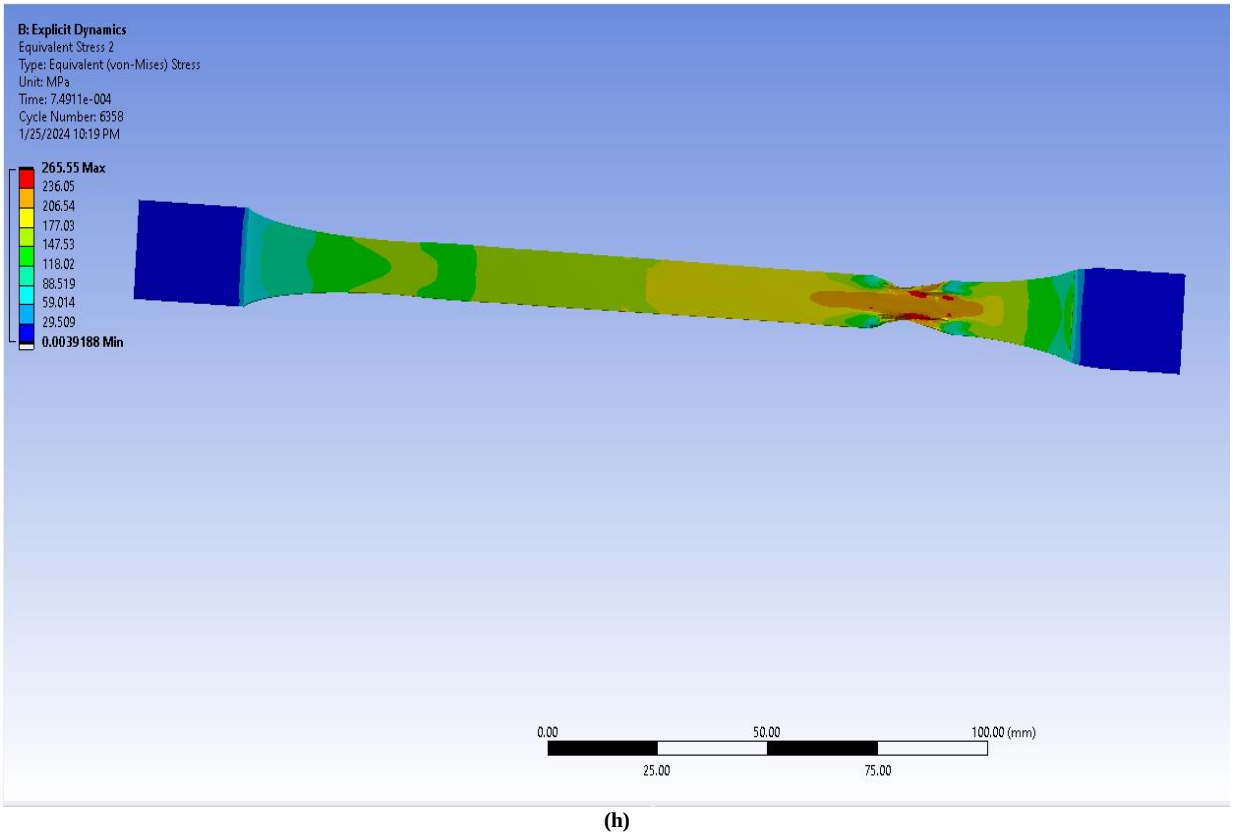

(h)

Fig. 10 Tensile simulation results for: (a) 2.5%wt MMT of 75µm particulate size, (b) 2.5%wt MMT of 100µm particulate size, (c) 5%wt MMT of 75µm particulate size, (d) 5%wt MMT of 100µm particulate size, (e) 7.5%wt MMT of 75µm particulate size, (f) 7.5%wt MMT of 100µm particulate size, (g) 10%wt MMT of 75µm particulate size, (h) 10%wt MMT of 100µm particulate size

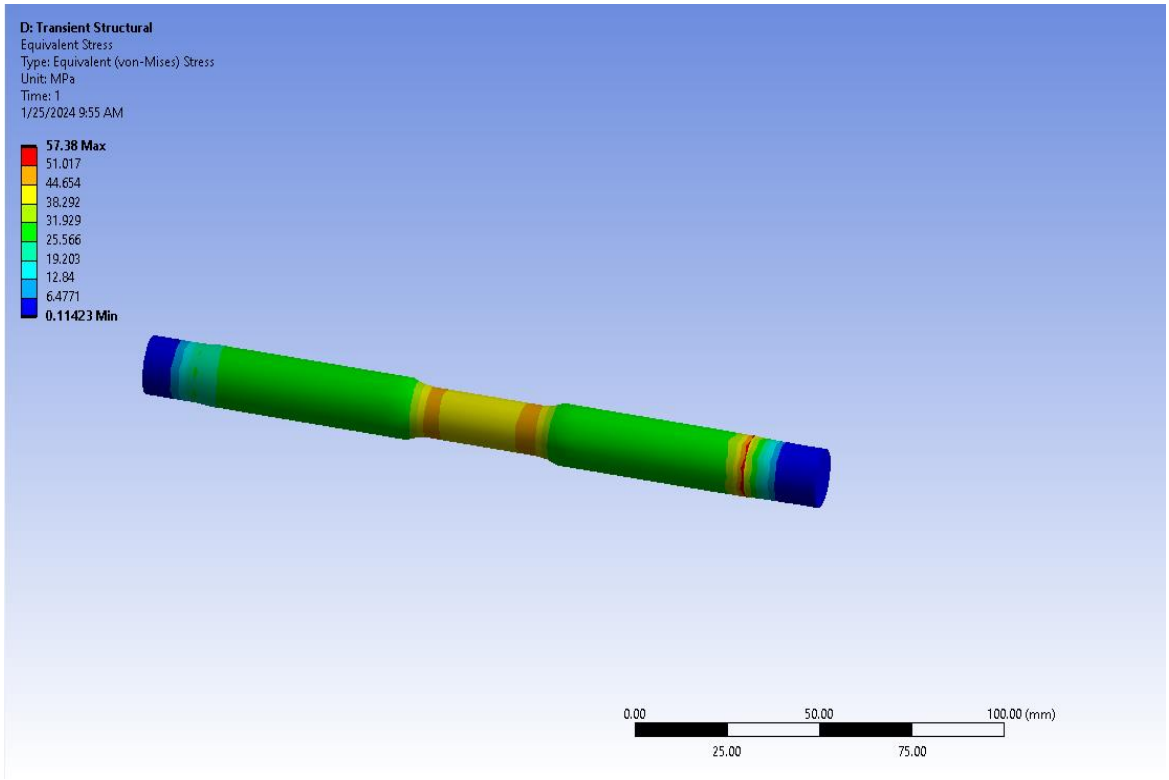
D: Transient Structural
Equivalent Stress
Type: Equivalent (von-Mises) Stress
Unit: MPa
Time: 1
1/25/2024 9:55 AM
57.38 Max
51.017
44.654
38.292
31.929
25.566
19.203
12.84
6.4771
0.11423 Min
0.00
50.00
100.00 (mm)
25.00
75.00

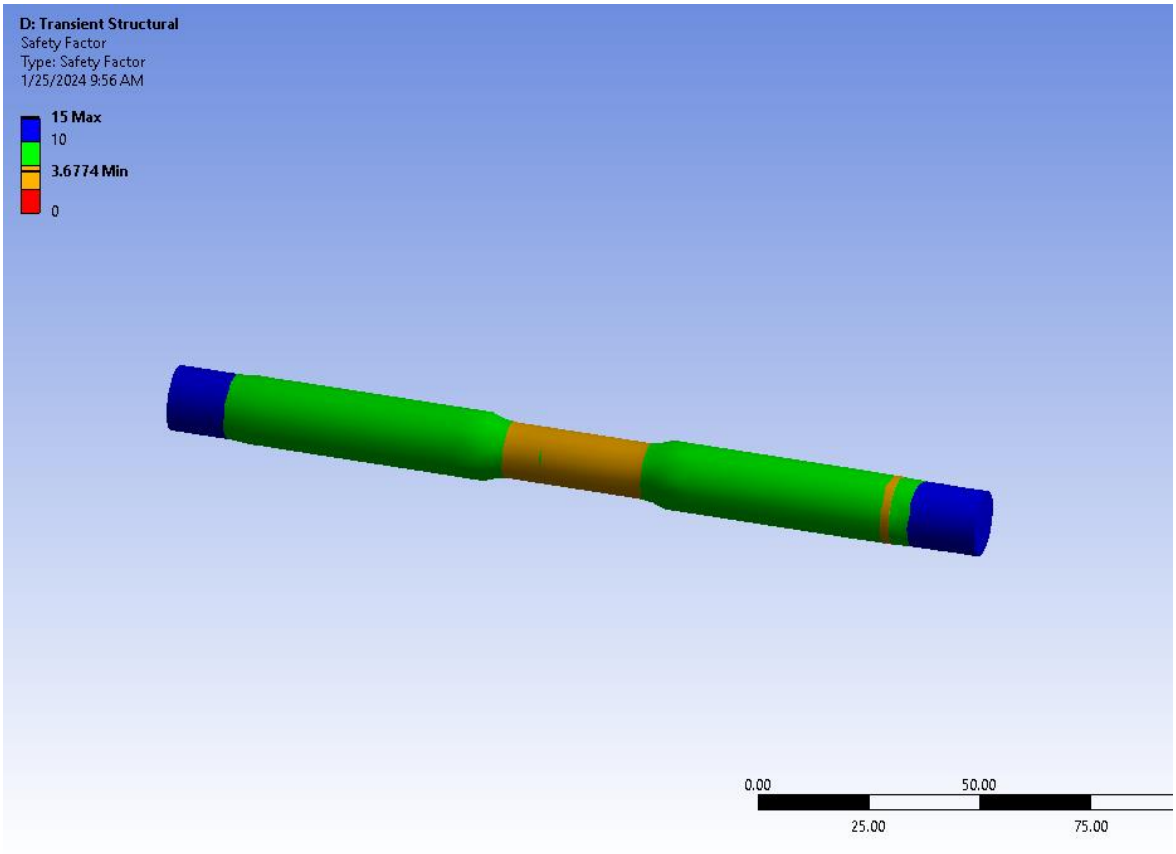
D: Transient Structural
Safety Factor
Type: Safety Factor
1/25/2024 9:56 AM
15 Max
10
3.6774 Min
0
0.00
50.00
25.00
75.00

(a)

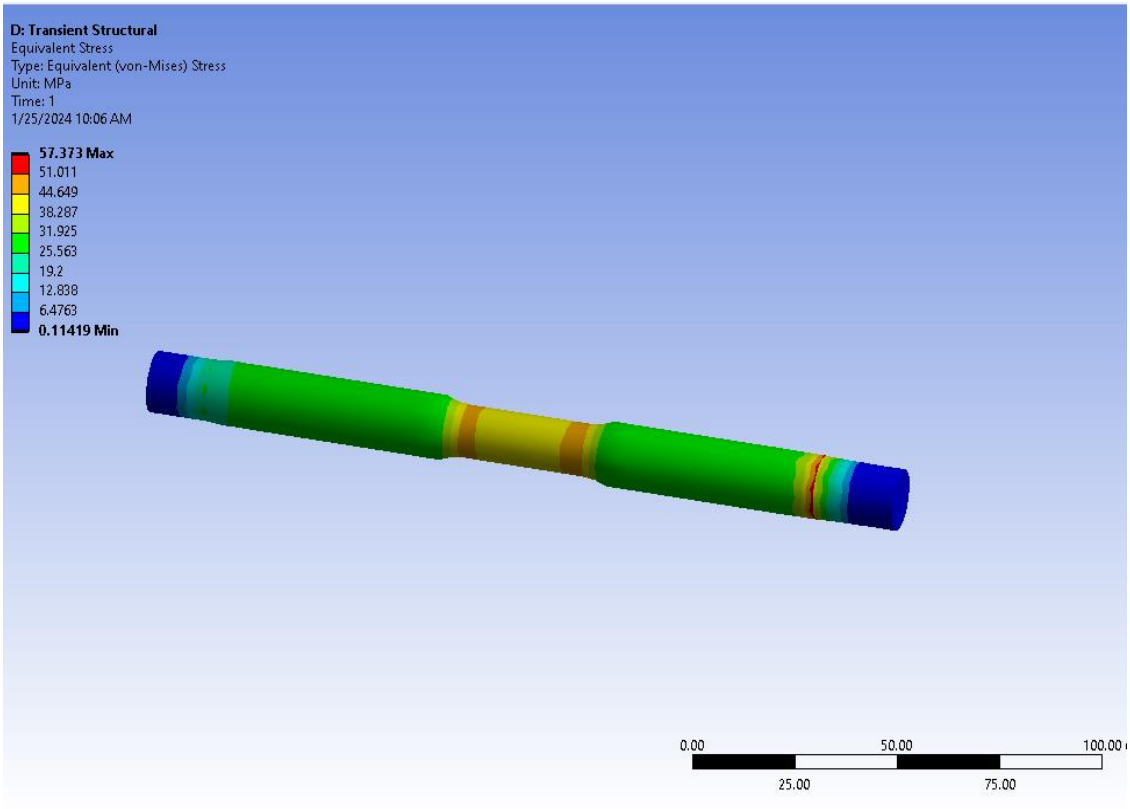
D: Transient Structural
Equivalent Stress
Type: Equivalent (von-Mises) Stress
Unit: MPa
Time: 1
1/25/2024 10:06 AM
57.373 Max
51.011
44.649
38.287
31.925
25.563
19.2
12.838
6.4763
0.11419 Min
0.00
50.00
100.00
25.00
75.00

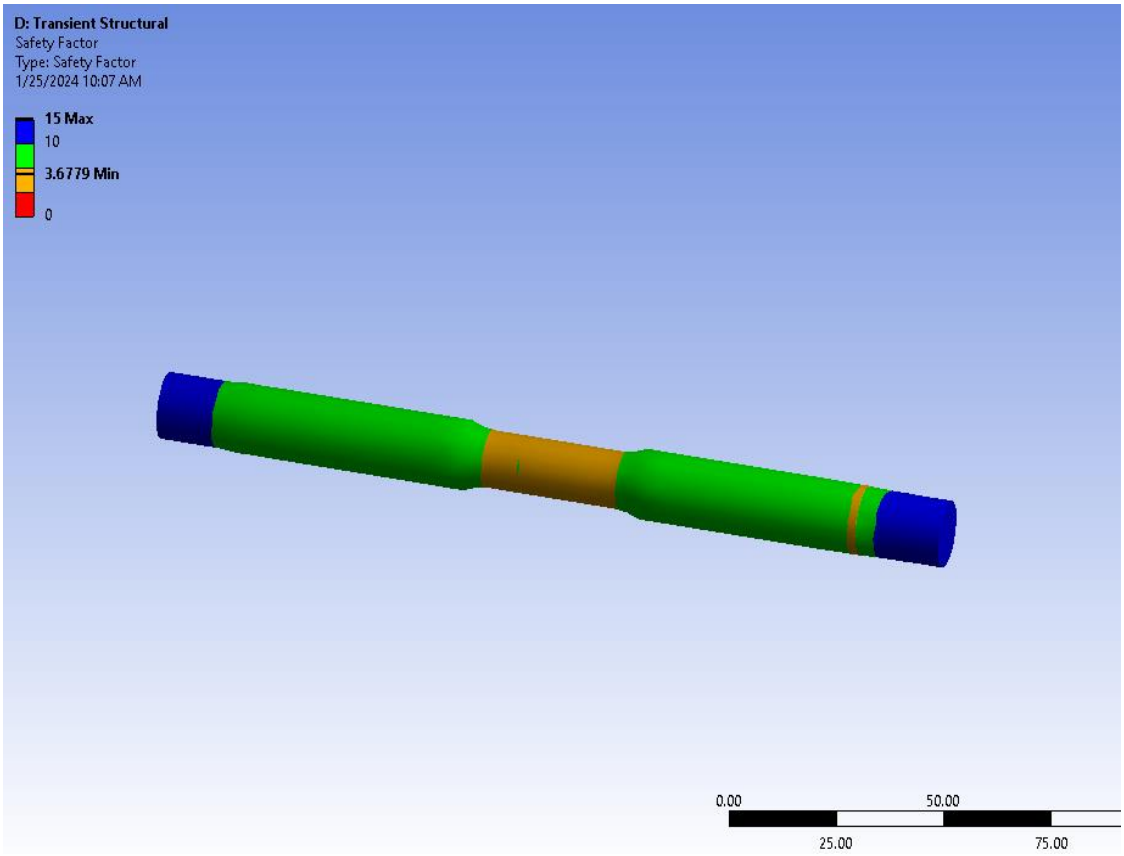
D: Transient Structural
Safety Factor
Type: Safety Factor
1/25/2024 10:07 AM
15 Max
10
3.6779 Min
0
0.00
50.00
25.00
75.00

(b)

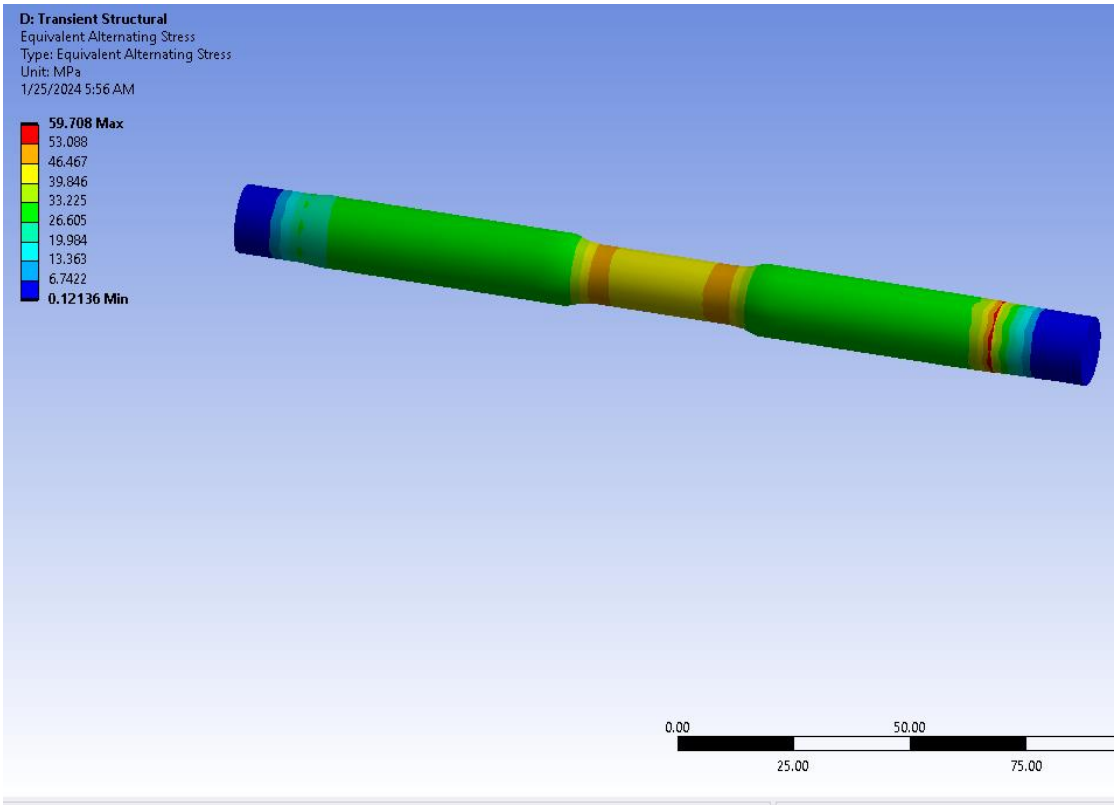
D: Transient Structural
Equivalent Alternating Stress
Type: Equivalent Alternating Stress
Unit: MPa
1/25/2024 5:56 AM
59.708 Max
53.088
46.467
39.846
33.225
26.605
19.984
13.363
6.7422
0.12136 Min
0.00
50.00
25.00
75.00

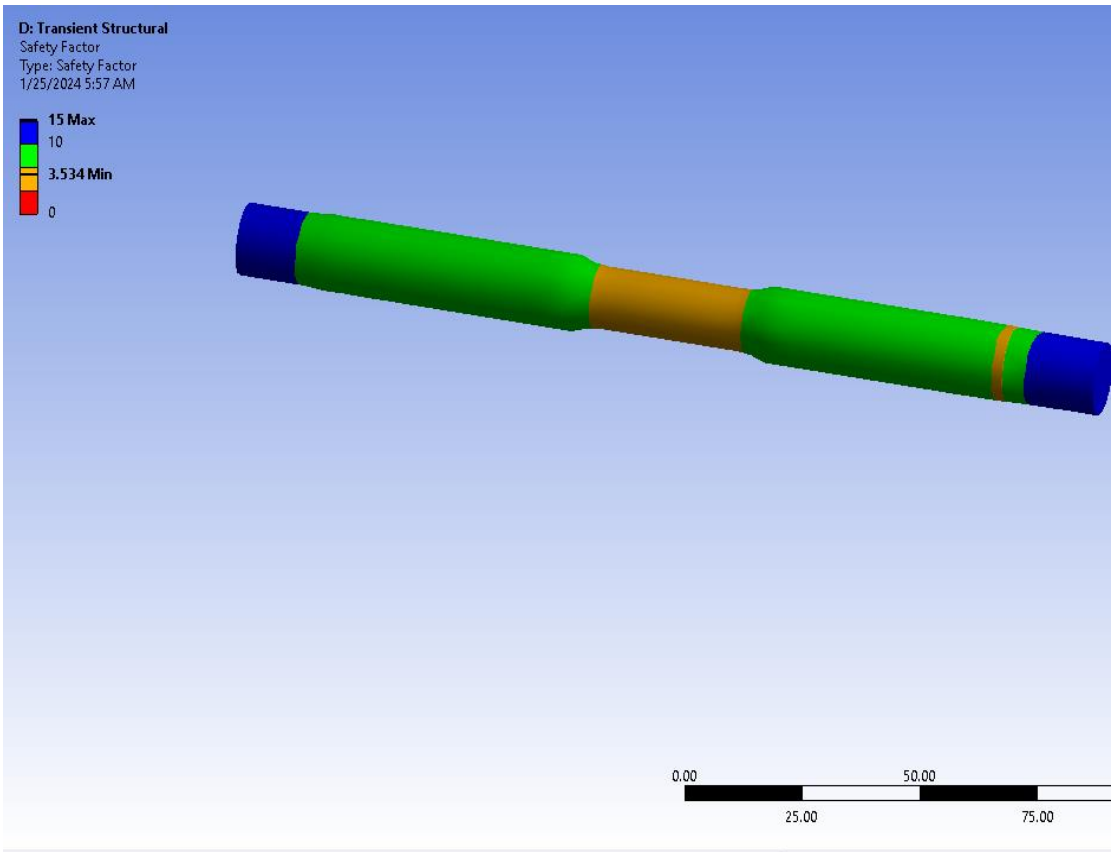
D: Transient Structural
Safety Factor
Type: Safety Factor
1/25/2024 5:57 AM
15 Max
10
3.534 Min
0
0.00
50.00
25.00
75.00

(c)

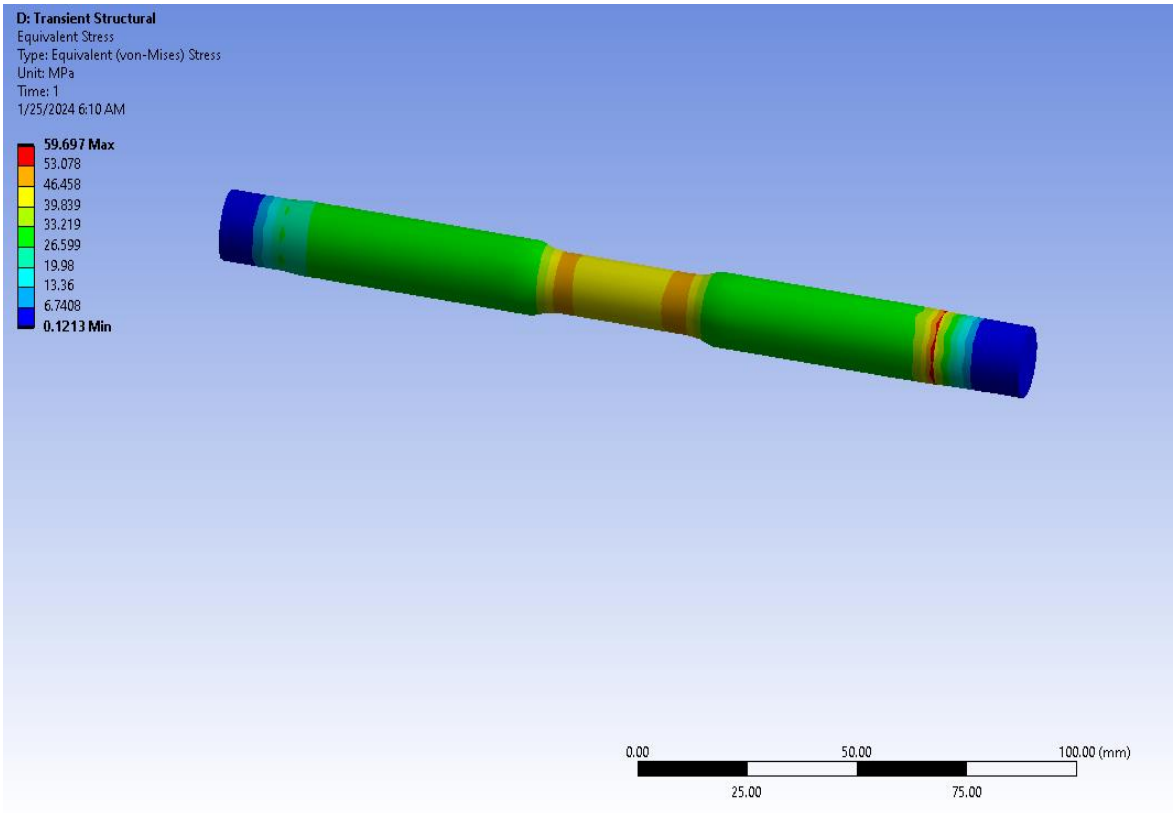
D: Transient Structural
Equivalent Stress
Type: Equivalent (von-Mises) Stress
Unit: MPa
Time: 1
1/25/2024 6:10 AM
59.697 Max
53.078
46.458
39.839
33.219
26.599
19.98
13.36
6.7408
0.1213 Min
0.00
50.00
100.00 (mm)
25.00
75.00

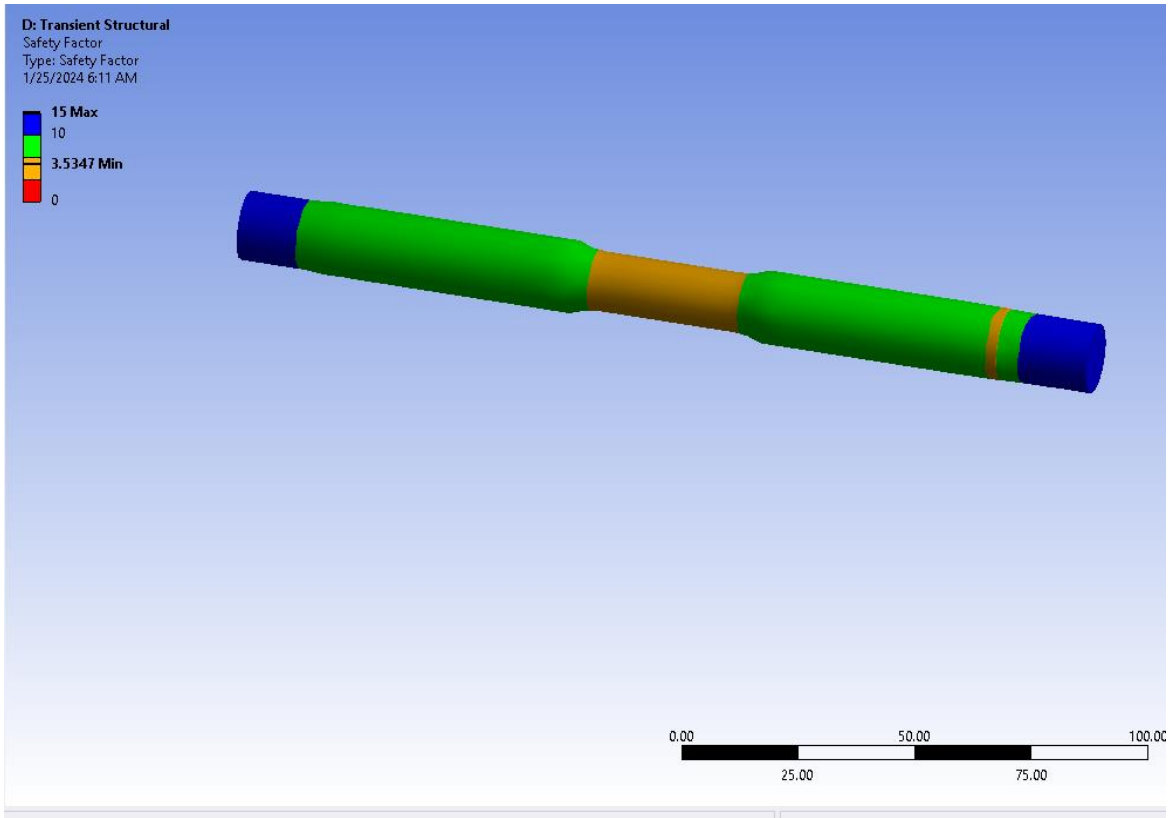
D: Transient Structural
Safety Factor
Type: Safety Factor
1/25/2024 6:11 AM
15 Max
10
3.5347 Min
0
0.00
50.00
100.00
25.00
75.00

(d)

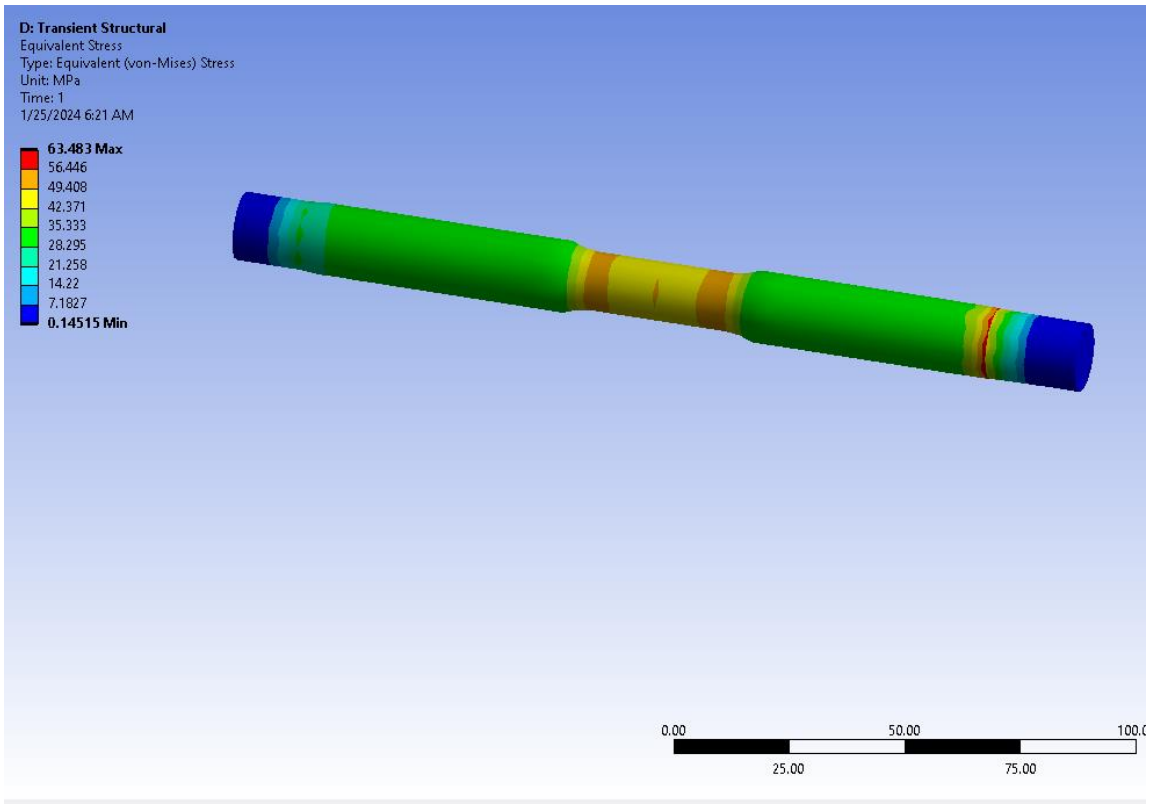
D: Transient Structural
Equivalent Stress
Type: Equivalent (von-Mises) Stress
Unit: MPa
Time: 1
1/25/2024 6:21 AM
63.483 Max
56.446
49.408
42.371
35.333
28.295
21.258
14.22
7.1827
0.14515 Min
0.00
50.00
25.00
75.00

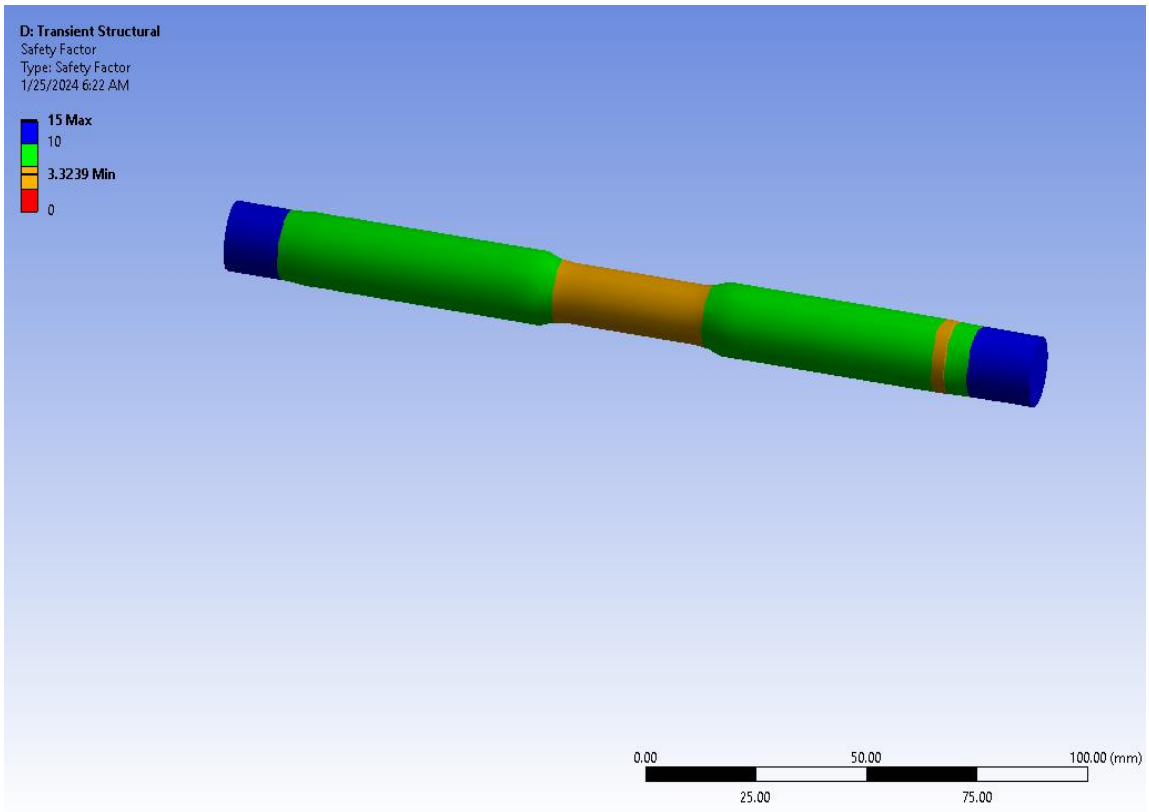
D: Transient Structural
Safety Factor
Type: Safety Factor
1/25/2024 6:22 AM
15 Max
10
3.3239 Min
0
0.00
50.00
100.00 (mm)
25.00
75.00

(e)

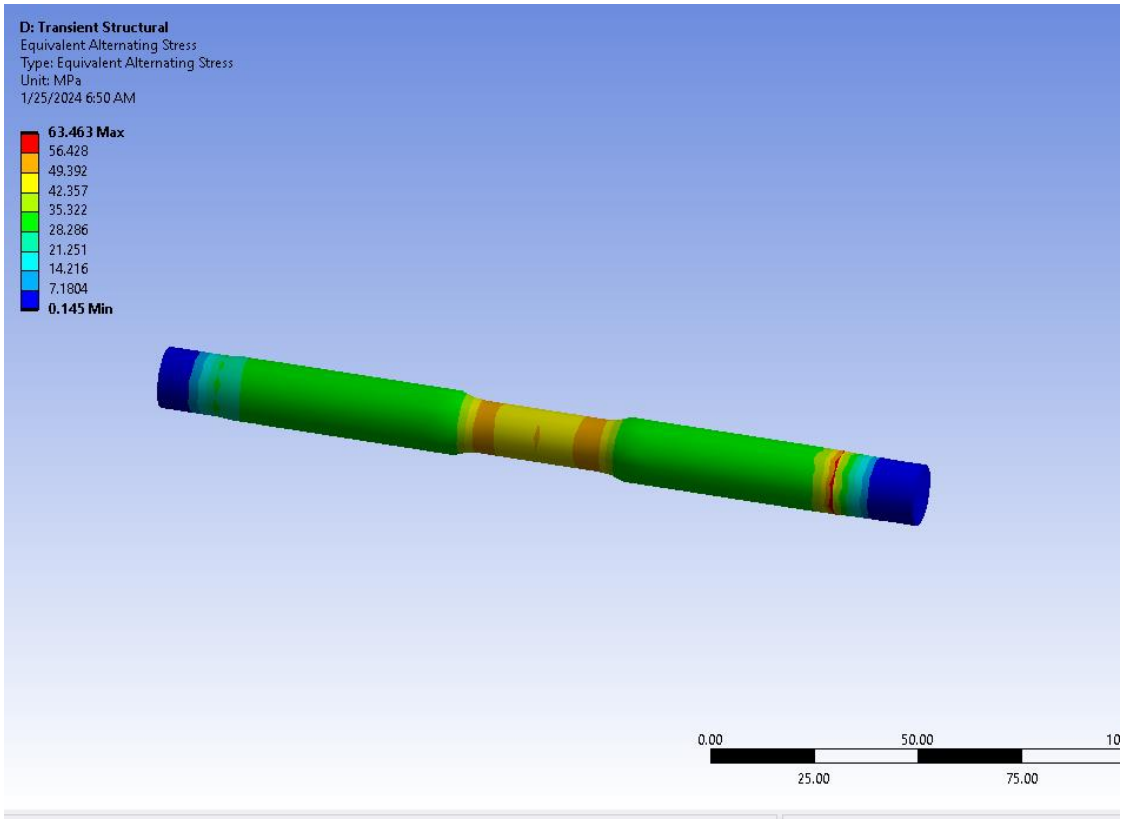
D: Transient Structural
Equivalent Alternating Stress
Type: Equivalent Alternating Stress
Unit: MPa
1/25/2024 6:50 AM
63.463 Max
56.428
49.392
42.357
35.322
28.286
21.251
14.216
7.1804
0.145 Min
0.00
50.00
25.00
75.00

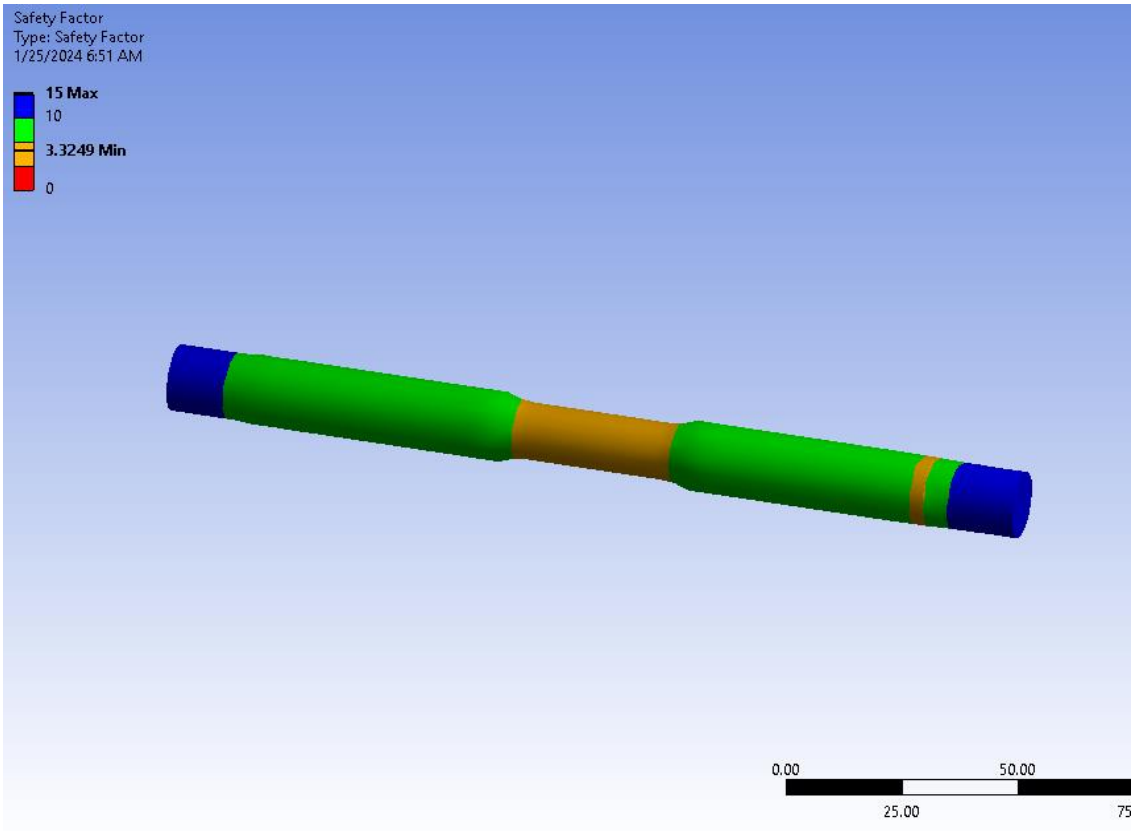
Safety Factor
Type: Safety Factor
1/25/2024 6:51 AM
15 Max
10
3.3249 Min
0
0.00
50.00
25.00

(f)

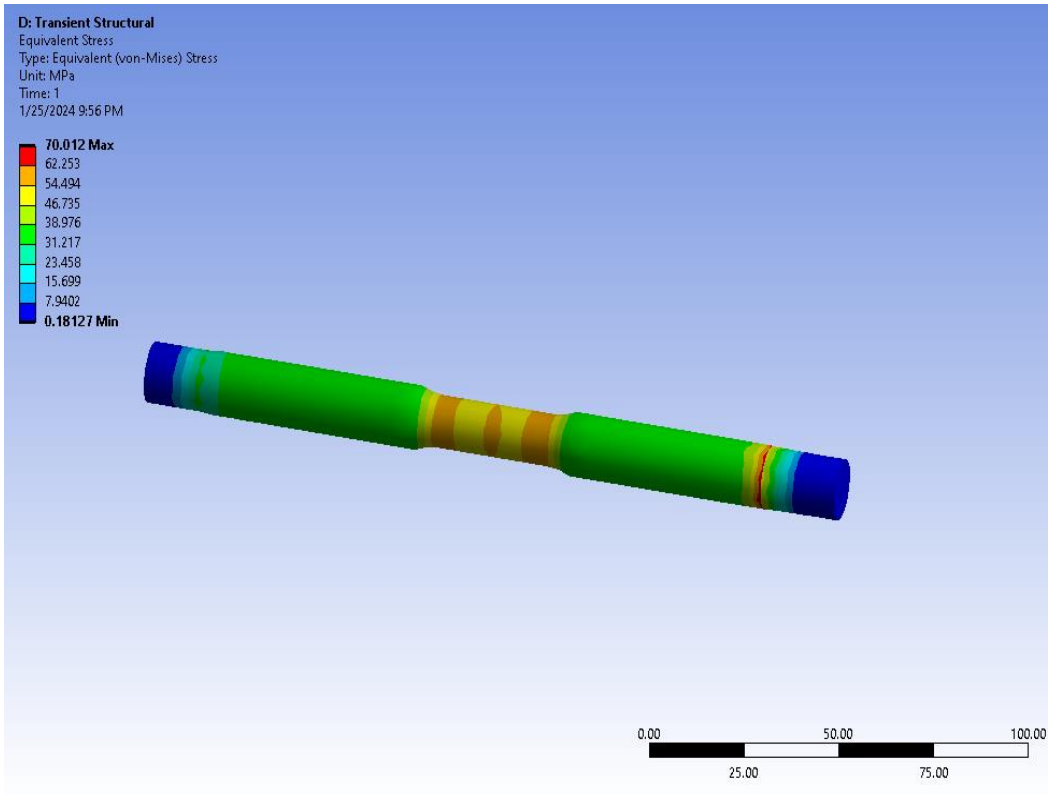
D: Transient Structural
Equivalent Stress
Type: Equivalent (von-Mises) Stress
Unit: MPa
Time: 1
1/25/2024 9:56 PM
70.012 Max
62.253
54.494
46.735
38.976
31.217
23.458
15.699
7.9402
0.18127 Min
0.00
50.00
100.00
25.00
75.00

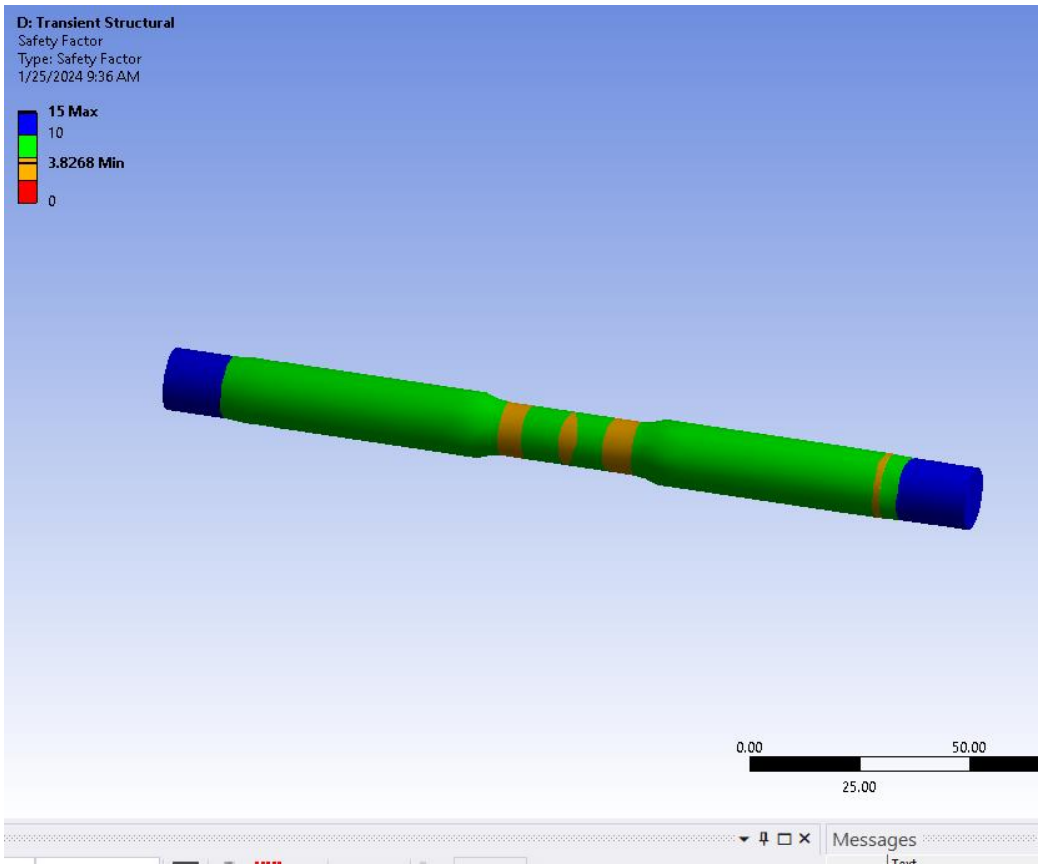
D: Transient Structural
Safety Factor
Type: Safety Factor
1/25/2024 9:36 AM
15 Max
10
3.8268 Min
0
0.00
50.00
25.00
Messages

(g)

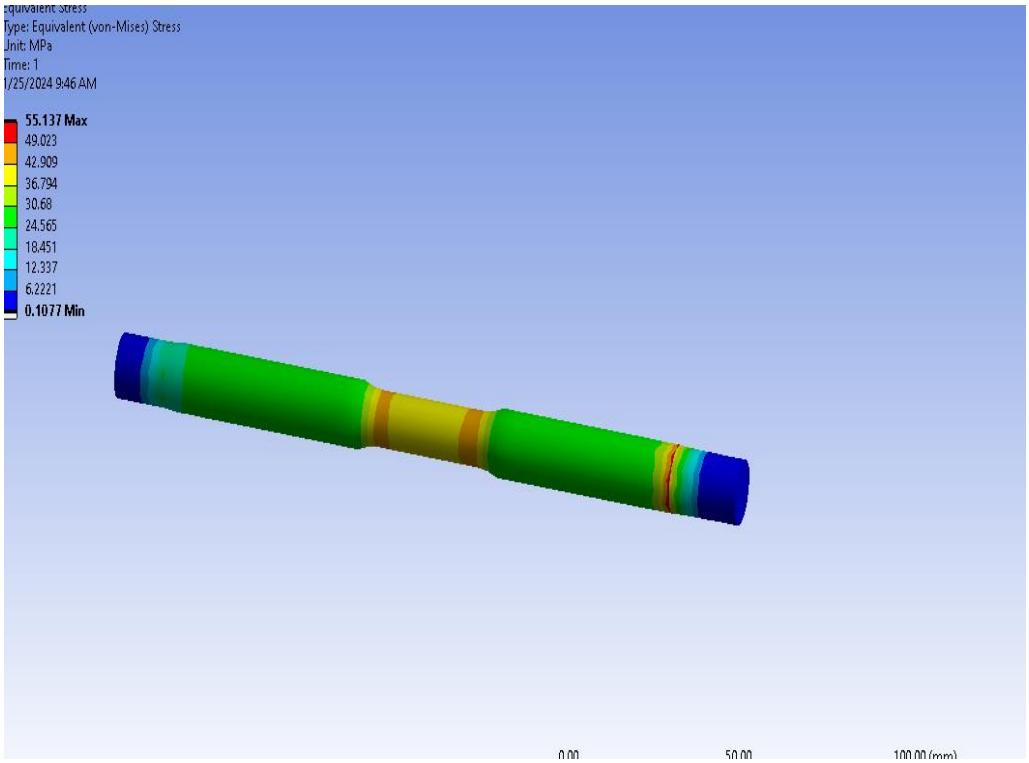

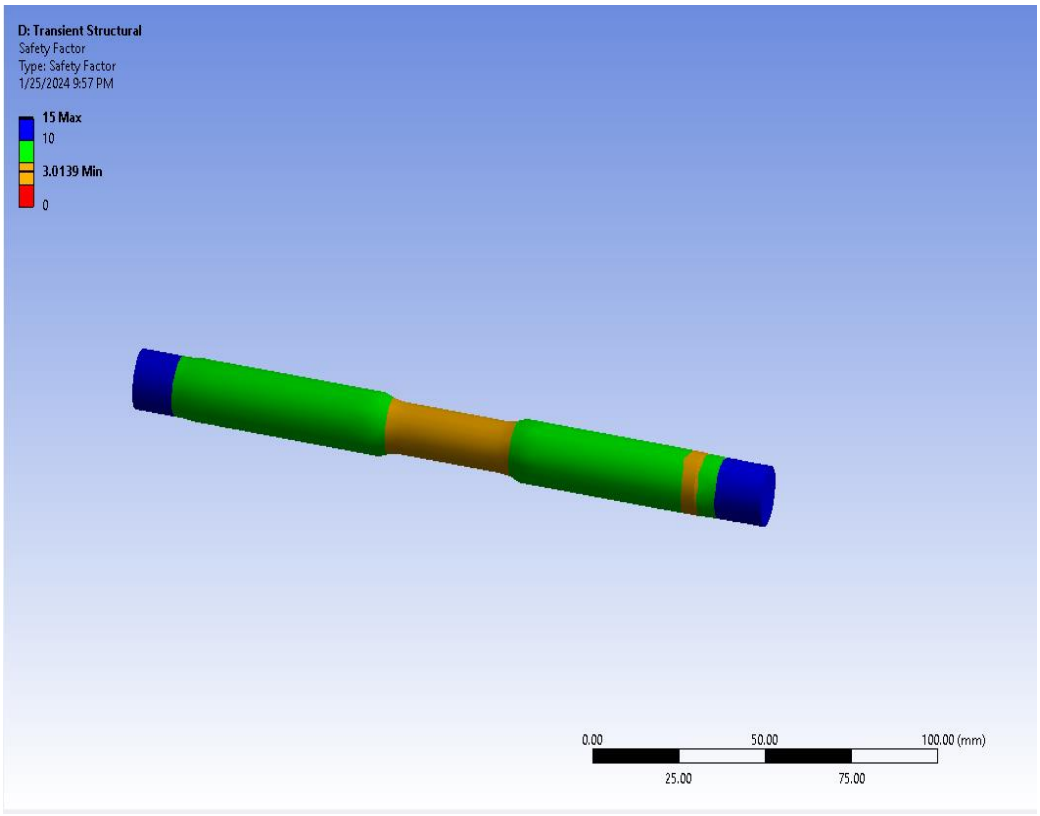

(h)

Fig. 11 Fatigue including the safety of factor simulation results for: (a) 2.5%wt MMT of 75µm particulate size, (b) 2.5%wt MMT of 100µm particulate size, (c) 5%wt MMT of 75µm particulate size, (d) 5%wt MMT of 100µm particulate size, (e) 7.5%wt MMT of 75µm particulate size, (f) 7.5%wt MMT of 100µm particulate size, (g) 10%wt MMT of 75µm particulate size, (h) 10%wt MMT of 100µm particulate size

3.4.1. Probability Plots

The probability plots evaluate the distribution of the obtained data, as represented in Table 6. Anderson Darling (ADT) test was used to verify the normality assumption [43]. The plotting in Figure 12 reflects that the data for all the responses lies close to the fitted line, and the ADT statics values are relatively low. The test p-value is greater than 0.05. Hence, the data is taken to have a normal distribution. This allows for more analysis and optimization of the data.

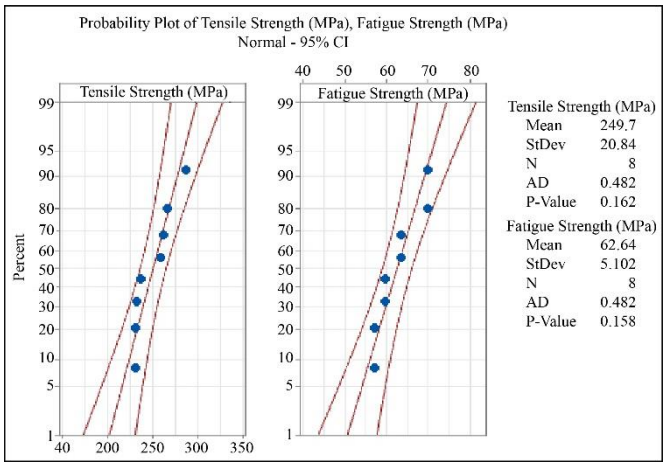

Fig. 12 Probability plots

3.4.2. Main Effect Plots of Means for Individual Response

Most composite materials have their tensile properties generally influenced by the filler content, and as the filler amount increases, so does the mechanical performance. Figure 13 (a) shows the main effect plots for tensile strength. It shows that tensile strength increases with an increase in MMT composition and decreases with an increase in MMT particulate size from low to high, i.e., 5% to 10% and 75 to 100 µm, respectively. Similarly, Figure 13(b) shows that fatigue strength increases with increased MMT composition. However, the MMT particulate size range has a minimal effect on fatigue strength.

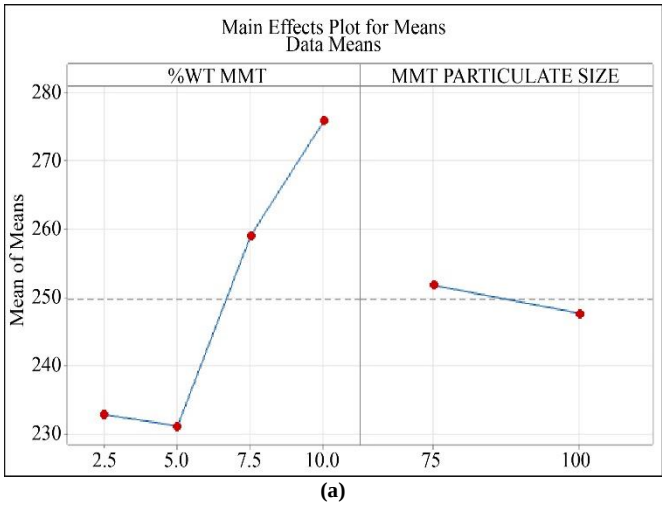

(a)

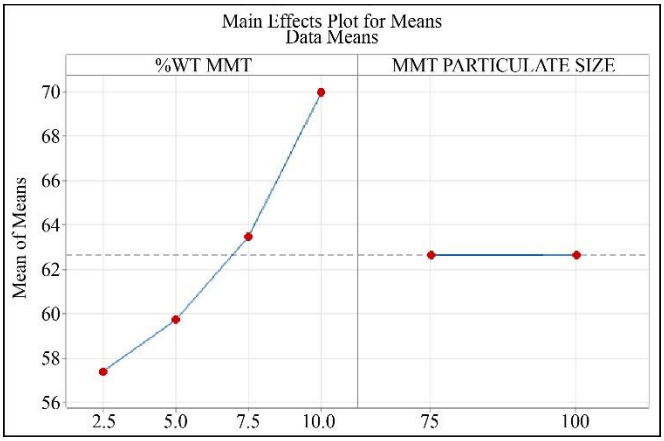

(b)

Fig. 13 (a)Plot of means for the tensile and (b)plot of means fatigue

3.5. SEM Analysis

Figure 14 shows an SEM micrograph of the cross-sectional surface of one of the filament samples with a magnification of 200×. It is noted that MMT is well dispersed in the polymer matrix, and some agglomerate formations were identified. The micrographs reinforce the possibility of good MMT dispersion in the rLDPE. Certain irregular formations depict the interaction between rLDPE and montmorillonite in the rLDPE/MMT composite. MMT is a hydrophilic clay that weakly interacts with the hydrophobic polymer-like rLDPE. Thus, the MMT tends to form some aggregated particles seen in the images. Similar findings have been observed and discussed in previous research studies. This structural interaction presents a possibility of inoculation with drugs for elution.

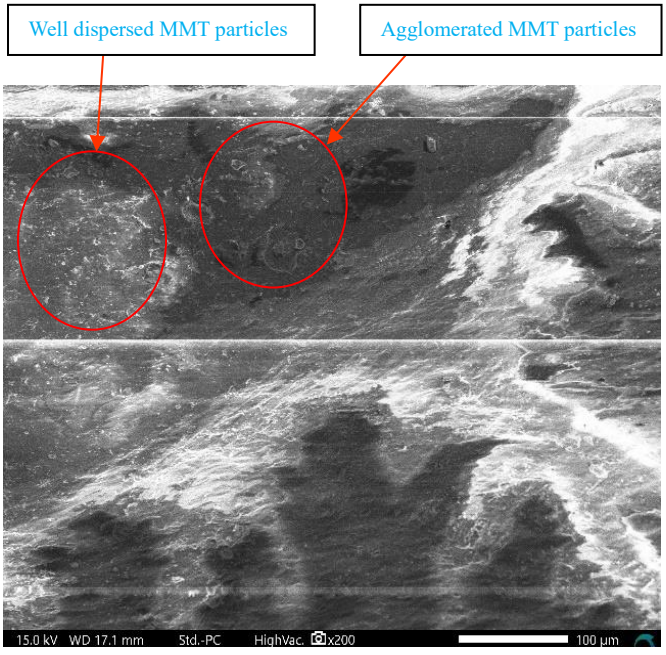

Fig. 14 Scanning electron microscope micrograph

3.6. Mechanical Test for Printed Samples

Physical samples were printed using fused deposition modeling, a 3D printing technique. Printing with rLDPE/MMT composite filament was challenging due to frequent clogging of the printer nozzle, deformation when cooling, and poor bed adhesion, leading to warping during the printing process. The P-surface 141 print sheet improved the part adhesion to the printing surface. In addition, brims promoted bed adhesion further and prevented warping. The other challenge was the inconsistent ovality of the filament, affecting the filament flow rate in the extrusion head.

3.6.1. Tensile Test

The maximum ultimate tensile strength obtained from the experiments was low. This could be due to the degradation of the polymers as a result of heating during filament fabrication and printing processes. Additionally, the sample fabrication technique used, Fused Deposition Modelling, gives a sample with a layer-based structure. This lowers the tensile strength compared to those processed through other methods, such as injection molding. This can be addressed by further optimization of manufacturing processes and parameters**.** Table 7 and Figure 15 shows the tensile results obtained from the tensile tests.

Table 7. Tensile test results

Name	Max. Force (N)	Max. Stress (N/mm^2)	Max. Disp. (MM)
Sample 1	75.695	1.328	4.696
Sample 2	56.130	0.985	5.150
Sample 3	41.097	0.721	6.168
Sample 4	38.813	0.681	9.540
Sample 5	140.359	2.462	9.312
Average	70.419	1.235	6.973

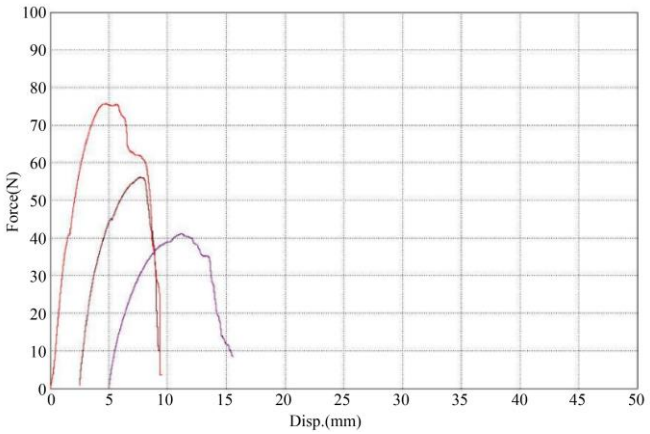

Fig. 15 Force displacement graph of the first three tensile test samples

3.6.2. Fatigue Test

The composite withstood 106 cycles of repeated bending stress of 15.03 MPa and a frequency of 36 Hz before failure. This is a high number of cycles, demonstrating the composite's strong fatigue resistance under cyclic bending loads. This is a crucial property for materials used in dynamic environments like drug-eluting stents (DES), which are subject to constant mechanical stress due to blood flow and pulsating pressure in the coronary arteries.

The composite failing at a stress level much higher than the maximum arterial pressure, approximately 0.02MPa (140 mmHg), implies that the rLDPE/MMT composite would not experience failure under the normal physiological pressures found in the human body. Further improvements in 3D printing parameters could enhance this performance and durability in real-world medical applications.

3.7. Composite Properties Influence Drug Release Rates

The rLDPE/MMT composite presents an enhanced drug delivery avenue for DES, with properties comparable to existing technologies. Montmorillonite is widespread for its adsorption and sustained drug-release properties. Previous studies confirm its ability to enhance hydrophobic drugs' dissolution rate and bioavailability, forming composites with polymeric materials [28],[44]. The intercalation of drugs within its layers allows for controlled release mechanisms; the drug molecules can be released gradually through diffusion and desorption processes [45],[46]. Furthermore, its incorporation into polymer matrices reduces initial burst release, promoting a more sustained release profile necessary for maintaining therapeutic drug levels over extended periods [45],[47].

The drug release kinetics of rLDPE/MMT composites can also be tailored by tuning the components and loading of the drug. Incorporating MMT enhances the mechanical properties of the composite and modifies its drug-release behavior. This is due to its thickening properties and electrostatic interactions with drug molecules [48],[49]. This is significant in the need for controlled drug delivery in stent applications, where maintaining a consistent drug concentration is essential to prevent restenosis.

Comparatively, existing DES technologies utilize polymeric coatings capable of releasing drugs through diffusion. However, these systems may be limited by rapid initial release and insufficient control over the release profile [50]. The rLDPE/MMT composites could potentially offer improved performance by leveraging the unique properties of MMT to provide a more predictable and sustained release of therapeutic agents. For example, the use of MMT in drug delivery systems has been associated with non-Fickian release mechanisms, which is beneficial for achieving desired pharmacokinetic profiles [51],[52].

Additionally, the mechanical stability and biocompatibility of rLDPE/MMT composites can be advantageous, as the materials must withstand physiological conditions while minimizing adverse reactions [53],[54]. The

ability to fine-tune the drug release rates by manipulating composite properties presents a significant advantage over traditional drug-eluting stent technologies, which may not offer the same level of customization.

In summary, the properties of recycled LDPE and montmorillonite composites play a crucial role in influencing drug release rates, offering a viable alternative to existing drug-eluting stent technologies. The unique characteristics of montmorillonite, combined with the mechanical properties of LDPE, enable the development of advanced drug delivery systems that can provide sustained and controlled release, thereby enhancing therapeutic efficacy and patient outcomes.

3.8. Scalability of 3D Printing Processes for Mass Production of Stents

The 3D printing processes can be scaled for the mass production of stents, which is currently gaining relevance in biomedical engineering. Integration of advanced 3D printing technologies can revolutionize the manufacturing of stents, enabling customized designs and cutting production times and costs.

3D printing technologies, based on stereolithography and other photopolymerization techniques, have been shown to produce patient-specific medical devices, including stents. Zhao et al. highlighted a homemade 3D printing system's effectiveness in fabricating various stent structures, demonstrating the potential for customization and rapid prototyping in clinical settings [55]. Similarly, Misra et al. developed a multidrug-eluting stent using a graphene-nanoplatelet-doped biodegradable polymer composite, showcasing the ability to tailor stent properties for improved patient outcomes [56]. These advancements indicate that 3D printing can facilitate the production of stents that are customized to individual patient anatomies and incorporate advanced materials for enhanced functionality.

Moreover, the scalability of 3D printing processes is supported by the ability to produce stents on demand, which can significantly reduce inventory costs and waste associated with traditional manufacturing methods. Lith et al. discussed using micro-continuous liquid interface production (microCLIP) to create high-resolution, bioresorbable vascular stents, emphasizing the speed and efficiency of this method [57]. This capability aligns with the growing demand for personalized medical devices, as it allows for rapid adaptation to patient needs without the extensive lead times typical of conventional manufacturing processes [58]. The flexibility of 3D printing technologies enables manufacturers to quickly pivot production lines in response to changing clinical requirements, as noted by Manero et al. in their review of 3D printing applications during the COVID-19 pandemic [59].

However, while the potential for scalability is evident, several challenges remain. Regulatory hurdles associated with the approval of 3D-printed medical devices can impede the widespread adoption of these technologies. Beitler et al. pointed out that establishing point-of-care (PoC) 3D printing centers has blurred the lines between healthcare providers and manufacturers, creating regulatory ambiguities that must be addressed to facilitate broader implementation [60]. Additionally, the need for standardized protocols in producing and testing 3D-printed stents is critical to ensure safety and efficacy, as highlighted by Kermavnar et al. in their systematic review [61].

In conclusion, the scalability of 3D printing processes for the mass production of stents presents a promising avenue for innovation in medical device manufacturing. The ability to produce customized, patient-specific stents rapidly and efficiently is a significant advantage over traditional methods. However, addressing regulatory challenges and establishing standardized production protocols will be essential for realizing the full potential of 3D printing in this field.

4. Conclusion

Recycled low-density polyethylene montmorillonite polymer composites were formulated, simulated, and test samples prepared through the FDM 3D printing technique and characterized by mechanical tests and SEM studies with individual compositing material characterized by FTIR and XRF. From the preceding discussion:

1. The results of this study show the feasibility of reusing and recycling polymer waste (recycled low-density polyethylene) for developing nanocomposites with good mechanical and morphological characteristics. This aligns with environmental sustainability by reducing plastic waste and offering a cost-effective alternative to virgin polymers, making DES more accessible while promoting a circular economy.
2. The composite can be simulated, optimized, and engineered for specific mechanical and pharmacokinetic needs, creating next-generation, patient-specific DES. This approach supports innovation in stent technology, with the potential for scalable, customizable, and multifunctional applications.
3. Both rLDPE and MMT are known for their biocompatibility, with their excellent interaction observed through the SEM micrographs, forming a homogeneous composite with good mechanical properties, making them suitable for biomedical applications and alternative materials for drug-eluting stents. The biocompatibility of the composite ensures that it does not induce adverse immune responses, inflammation, or thrombosis, which are common concerns in DES materials.

The formulation, simulation, optimization, development, and evaluation of a biopolymer composite from recycled low-density polyethylene (rLDPE) and montmorillonite (MMT)

for drug-eluting stents are justified by the potential to achieve an optimal balance between sustainability, mechanical performance, biocompatibility, and controlled drug release. This approach addresses the current limitations of DES materials and supports the development of cost-effective, environmentally friendly, and customizable stent technologies.

Future research should focus on comprehensive in vitro studies to further evaluate the long-term biocompatibility and biodegradation behavior of rLDPE/MMT composites and explore strategies to optimize their drug-release profile. Additionally, industrial and academic collaboration is needed to accelerate the development and adoption of sustainable materials in DES through industry-sponsored research projects, early-stage prototype testing, and feedback from clinicians on the practical requirements for DES materials.

Acknowledgments

The authors gratefully acknowledge PAUSTI and JKUAT for their support and institutional facilities in fulfilling this work.

Funding

The authors thank the African Union Commission for Education, Science, Technology, and Innovation for providing financial support for this research.

References

[1] Fatemeh Ahadi et al., "Evaluation of Coronary Stents: A Review of Types, Materials, Processing Techniques, Design, and Problems," *Heliyon*, vol. 9, no. 2, 2023. [CrossRef] [Google Scholar] [Publisher Link]

[2] Claudiu N. Lungu, Andreea Creteanu, and Mihaela C. Mehedinti, "Endovascular Drug Delivery," *Life*, vol. 14, no. 4, pp. 1-39, 2024. [CrossRef] [Google Scholar] [Publisher Link]

[3] I. Rykowska, I. Nowak, and R. Nowak, "Drug-Eluting Stents and Balloons-Materials, Structure Designs, and Coating Techniques: A Review," *Molecules*, vol. 25, no. 20, pp. 1-52, 2020. [CrossRef] [Google Scholar] [Publisher Link]

[4] Natalia Beshchasna et al., "Recent Advances in Manufacturing Innovative Stents," *Pharmaceutics*, vol. 12, no. 4, pp. 1-36, 2020. [CrossRef] [Google Scholar] [Publisher Link]

[5] B. Polanec, J. Kramberger, and S. Glodez, "A Review of Production Technologies and Materials for Manufacturing of Cardiovascular Stents," *Advances in Production Engineering And Management*, vol. 15, no. 4, pp. 390-402, 2020. [CrossRef] [Google Scholar] [Publisher Link]

[6] Magesh Sankar et al., "Magnesium-Based Alloys and Nanocomposites for Biomedical Application," *Applications of Nanocomposite Materials in Orthopedics*, pp. 83-109, 2019. [CrossRef] [Google Scholar] [Publisher Link]

[7] K. Milewski et al., "Comparison of Thin-Strut Cobalt-Chromium Stents and Stainless Steel Stents in a Porcine Model of Neointimal Hyperplasia," *Medical Science Monitor*, vol. 16, no. 1, 2010. [CrossRef] [Google Scholar] [Publisher Link]

[8] Ian B. A. Menown et al., "The Platinum Chromium Element Stent Platform: From Alloy, To Design, to Clinical Practice," *Advances in Therapy*, vol. 27, pp. 129-141, 2010. [CrossRef] [Google Scholar] [Publisher Link]

[9] Jiayin Fu et al., "Evolution of Metallic Cardiovascular Stent Materials: A Comparative Study Among Stainless Steel, Magnesium and Zinc," *Biomaterials*, vol. 230, 2020. [CrossRef] [Google Scholar] [Publisher Link]

[10] Ahsan Riaz Khan et al., "Recent Advances in Biodegradable Metals for Implant Applications: Exploring in Vivo and in Vitro Responses," *Results in Engineering*, vol. 20, pp. 1-16, 2023. [CrossRef] [Google Scholar] [Publisher Link]

[11] Shukufe Amukarimi, and Masoud Mozafari, "Biodegradable Magnesium-Based Biomaterials: An Overview of Challenges and Opportunities," *MedComm*, vol. 2, no. 2, pp. 123-144, 2021. [CrossRef] [Google Scholar] [Publisher Link]

[12] Ling Ding et al., "Polymer-Based Drug Delivery Systems for Cancer Therapeutics," *Polymers*, vol. 16, no. 6, pp. 1-35, 2024. [CrossRef] [Google Scholar] [Publisher Link]

[13] Rasit Dinc, and Halit Yerebakan, "Atlas Drug-Eluting Coronary Stents Inhibit Neointimal Hyperplasia in Sheep Modeling," *Acta Cardiol Sin*, vol. 40, no. 5, pp. 585-594, 2024. [CrossRef] [Google Scholar] [Publisher Link]

[14] Arif A. Al Nooryani et al., "The Role of Optical Coherence Tomography Guidance in Scaffold Versus Stent Optimization," *The Egyptian Heart Journal*, vol. 72, no. 1, 2020. [CrossRef] [Google Scholar] [Publisher Link]

[15] Ta-Hsin Tsung et al., "Biodegradable Polymer-Based Drug-Delivery Systems for Ocular Diseases," *International Journal of Molecular Sciences*, vol. 24, no. 16, pp. 1-32, 2023. [CrossRef] [Google Scholar] [Publisher Link]

[16] Wei Xu, Makoto Sasaki, and Takuro Niidome, "Sirolimus Release from Biodegradable Polymers for Coronary Stent Application: A Review," *Pharmaceutics*, vol. 14, no. 3, pp.1-16, 2022. [CrossRef] [Google Scholar] [Publisher Link]

[17] Aydin Bordbar-Khiabani, and Michael Gasik, "Smart Hydrogels for Advanced Drug Delivery Systems," *International Journal of Molecular Sciences*, vol. 23, no. 7, pp. 1-23, 2022. [CrossRef] [Google Scholar] [Publisher Link]

[18] Stephanie Fuchs, Kaavian Shariati, and Minglin Ma, "Specialty Tough Hydrogels and Their Biomedical Applications," *Advanced Healthcare Materials*, vol. 9, no. 2, 2020. [CrossRef] [Google Scholar] [Publisher Link]

[19] Viritpon Srimaneepong et al., "Graphene for Antimicrobial and Coating Application," *International Journal of Molecular Sciences*, vol. 23, no. 1, pp. 1-17, 2022. [CrossRef] [Google Scholar] [Publisher Link]

[20] Keshav Narayan Alagarsamy et al., "Carbon Nanomaterials for Cardiovascular Theranostics: Promises and Challenges," *Bioactive Materials*, vol. 6, no. 8, pp. 2261-2280, 2021. [CrossRef] [Google Scholar] [Publisher Link]

[21] Lingling Ou et al., "Toxicity of Graphene-Family Nanoparticles: A General Review of the Origins and Mechanisms," *Part Fibre Toxicol*, vol. 13, pp. 1-24, 2016. [CrossRef] [Google Scholar] [Publisher Link]

[22] Jayanta Kumar Patra et al., "Nano Based Drug Delivery Systems: Recent Developments and Future Prospects," *Journal of Nanobiotechnology*, vol. 16, no. 1, pp. 1-33, 2018. [CrossRef] [Google Scholar] [Publisher Link]

[23] Asmaa M. Elsherbini, and Sally A. Sabra, "Nanoparticles-In-Nanofibers Composites: Emphasis on Some Recent Biomedical Applications," *Journal of Controlled Release*, vol. 348, pp. 57-83, 2022. [CrossRef] [Google Scholar] [Publisher Link]

[24] Lara Yildirimer et al., "Toxicology and Clinical Potential of Nanoparticles," *Nano Today*, vol. 6, no. 6, pp. 585-607, 2011. [CrossRef] [Google Scholar] [Publisher Link]

[25] Qing Li, and Yiu-Wing Mai, *Biomaterials for Implants and Scaffolds*, 1st ed., Springer Berlin, Heidelberg, pp. 1-466, 2017. [CrossRef] [Google Scholar] [Publisher Link]

[26] Chen Pan, Yafeng Han, and Jiping Lu, "Structural Design of Vascular Stents: A Review," *Micromachines*, vol. 12, no. 7, pp. 1-26, 2021. [CrossRef] [Google Scholar] [Publisher Link]

[27] Melissa Sgarioto et al., "Properties and in Vitro Evaluation of High Modulus Biodegradable Polyurethanes for Applications in Cardiovascular Stents," *Journal of Biomedical Materials Research Part B: Applied Biomaterials*, vol. 102, no. 8, pp. 1711-1719, 2014. [CrossRef] [Google Scholar] [Publisher Link]

[28] Ju-Hwan Park et al., "Application of Montmorillonite in Bentonite as a Pharmaceutical Excipient in Drug Delivery Systems," *Journal of Pharmaceutical Investigation*, vol. 46, no. 4, pp. 363-375, 2016. [CrossRef] [Google Scholar] [Publisher Link]

[29] Saprini Hamdiani et al., "Development of Green Composite Based on Recycled-Low Density Polyethylene (r-LDPE) as an Environmentally Friendly Packaging," *Pijar Mipa Journal*, vol. 19, no. 3, pp. 553-557, 2024. [CrossRef] [Google Scholar] [Publisher Link]

[30] Pamela Rodrigues Passos Severino et al., "Protective Low-Density Polyethylene Residues from Prepreg for the Development of New Nanocomposites with Montmorillonite: Recycling and Characterization," *Recycling*, vol. 4, no. 4, pp. 1-12, 2019. [CrossRef] [Google Scholar] [Publisher Link]

[31] Xiaohong Zhang et al., "Enhanced Breakdown Strength and Electrical Tree Resistance Properties of MMT/SiO_2 /LDPE Multielement Composites," *Journal of Applied Polymer Science*, vol. 136, no. 17, 2019. [CrossRef] [Google Scholar] [Publisher Link]

[32] Lijun Yang et al., "Electric Field Inducement of Montmorillonite in Ldpe and Properties of Electrical Tree Growing in this Composite," *IEEE Transactions on Dielectrics and Electrical Insulation*, vol. 22, no. 3, pp. 1684-1693, 2015. [CrossRef] [Google Scholar] [Publisher Link]

[33] Pamela Rodrigues Passos Severino et al., "The Use of Recycled Low-Density Polyethylene Films from Protective Prepreg for the Development of Nanocomposites with Bentonite Clay," *Journal of Applied Polymer Science*, vol. 138, no. 24, 2021. [CrossRef] [Google Scholar] [Publisher Link]

[34] Ruijin Liao et al., "Influence of Montmorillonite on Electrical Treeing and Breakdown Characteristics of Low-Density Polyethylene," *Journal of Reinforced Plastics and Composites*, vol. 33, no. 23, pp. 2117-2128, 2014. [CrossRef] [Google Scholar] [Publisher Link]

[35] M. Safa Bodur, Hasret E. Sonmez, and Mustafa Bakkal, "An Investigation for the Effect of Recycled Matrix on the Properties of Textile Waste Cotton Fiber Reinforced (T-FRP) Composites," *Polymer Composites*, vol. 38, no. 7, pp. 1231-1240, 2017. [CrossRef] [Google Scholar] [Publisher Link]

[36] ASTM E1252-98 "Standard Practice for General Techniques for Obtaining Infrared Spectra for Qualitative Analysis," *ASTM International West Conshohocken*, PA, USA, pp. 1-13, 2021. [CrossRef] [Google Scholar] [Publisher Link]

[37] ASTM "Standard Test Methods for Chemical Analysis of Hydraulic Cement," ASTM International, West Conshohocken, PA, USA, pp. 1-30, 2017. [CrossRef] [Google Scholar] [Publisher Link]

[38] Grace Njeri Wamuti et al., "Optimization of Extrusion Process Parameters of Recycled High-Density Polyethylene-Thermoplastic Starch Composite for Fused Filament Fabrication," *Open Journal of Composite Materials*, vol. 13, no. 4, pp. 69-86, 2023. [CrossRef] [Google Scholar] [Publisher Link]

[39] ASTM E2809-22, "Standard Guide for Using Scanning Electron Microscopy/Energy Dispersive X-Ray Spectroscopy (SEM/EDS) in Forensic Polymer Examinations," *ASTM International*, pp. 1-8, 2022. [CrossRef] [Publisher Link]

[40] Asep Bayu Dan Nandiyanto, Rosi Oktiani, and Risti Ragadhita, "How to Read and Interpret Ftir Spectroscope of Organic Material," *Indonesian Journal of Science and Technology*, vol. 4, no. 1, pp. 97-118, 2019. [Google Scholar] [Publisher Link]

[41] Zhiyu Yang et al., "Strengthening And Weakening Effects of Particles on Strength and Ductility of Sic Particle Reinforced Al-Cu-Mg Alloys Matrix Composites," *Materials*, vol. 14, no. 5, pp. 1-11, 2021. [CrossRef] [Google Scholar] [Publisher Link]

[42] A. Mamoon, and A. Al-Jaafari, "Fatigue Behavior of Aluminum Sic Nano Composites Material with Different Reinforcement Ratio," *IOP Conference Series: Materials Science and Engineering, The International Conference on Engineering and Advanced Technology (ICEAT 2020)*, Assiut, Egypt, vol .870, no. 1, pp. 1-11, 2020. [CrossRef] [Google Scholar] [Publisher Link]

[43] Mohsin Iqbal Qazi et al., "An Integrated Approach of GRA Coupled with Principal Component Analysis for Multi-Optimization of Shielded Metal Arc Welding (SMAW) Process," *Materials*, vol. 13, no. 16, pp. 1-22, 2020. [CrossRef] [Google Scholar] [Publisher Link]

[44] Xianfeng Yue et al., "Loading and Sustained Release of Benzyl Ammonium Chloride (BAC) in Nano-Clays," *Materials*, vol. 12, no. 22, pp. 1-12, 2019. [CrossRef] [Google Scholar] [Publisher Link]

[45] Ahmad Ainurofiq, and Syaiful Choiri, "Application of Montmorillonite, Zeolite and Hydrotalcite Nanocomposite Clays-Drug as Drug Carrier of Sustained Release Tablet Dosage Form," *Indonesian Journal of Pharmacy*, vol. 25, no. 3, pp. 125-131, 2014. [Google Scholar] [Publisher Link]

[46] Baohong Sun et al., "Study On Montmorillonite-Chlorhexidine Acetate-Terbinafine Hydrochloride Intercalation Composites as Drug Release Systems," *RSC Advances*, vol. 8, no. 38, pp. 21369-21377, 2018. [CrossRef] [Google Scholar] [Publisher Link]

[47] Vasudha Vaid Khushbu et al., "A Comparative Evaluation of Sustained Release of Chlorphenamine Based on a Nanocomposite of Chitosan, Pectin and Montmorillonite," *ChemistrySelect*, vol. 7, no. 14, 2022. [CrossRef] [Google Scholar] [Publisher Link]

[48] Valeria Ambrogi, Morena Nocchetti, and Loredana Latterini, "Promethazine-Montmorillonite Inclusion Complex To Enhance Drug Photostability," *Langmuir*, vol. 30, no. 48, pp. 14612-14620, 2014. [CrossRef] [Google Scholar] [Publisher Link]

[49] Nadia Elsayed, Mashari Elsharif, and Wael Sabry Mohamed, "Preparation and Characterization of Melt Spun Polypropylene / Montmorillonite Nanocomposite Fibre for Ibuprofen Drug Delivery Application," *Egyptian Journal of Chemistry*, vol. 61, no. 2, pp. 259-268, 2018. [CrossRef] [Google Scholar] [Publisher Link]

[50] Innocent J. Macha et al., "Marine Structure Derived Calcium Phosphate-Polymer Biocomposites for Local Antibiotic Delivery," *Marine Drugs*, vol. 13, no. 1, pp. 666-680, 2015. [CrossRef] [Google Scholar] [Publisher Link]

[51] Christopher J. Ward, Shang Song, and Edward W. Davis, "Controlled Release of Tetracycline-HCl from Halloysite-Polymer Composite Films," *Journal of Nanoscience and Nanotechnology*, vol. 10, no. 10, pp. 6641-6649, 2010. [CrossRef] [Google Scholar] [Publisher Link]

[52] Murilo L. Bello et al., "Sodium Montmorillonite/Amine-Containing Drugs Complexes: New Insights on Intercalated Drugs Arrangement into Layered Carrier Material," *PLoS One*, vol. 10, no. 3, 2015. [CrossRef] [Google Scholar] [Publisher Link]

[53] Xu Liu et al, "Clay-Polymer Nanocomposites Prepared by Reactive Melt Extrusion for Sustained Drug Release," *Pharmaceutics*, vol. 12, no. 1, pp. 1-23, 2020. [CrossRef] [Google Scholar] [Publisher Link]

[54] Angela Faccendini et al., "Norfloxacin-Loaded Electrospun Scaffolds: Montmorillonite Nanocomposite vs. Free Drug," *Pharmaceutics*, vol. 12, no. 4, pp. 1-24, 2020. [CrossRef] [Google Scholar] [Publisher Link]

[55] Hirotoshi Watanabe, Takenori Domei, and Takeshi Morimoto, "Effect of 1-Month Dual Antiplatelet Therapy Followed by Clopidogrel vs 12-Month Dual Antiplatelet Therapy on Cardiovascular and Bleeding Events in Patients Receiving PCI," *JAMA*, vol. 321, no. 24, pp. 2414-2427, 2019. [CrossRef] [Google Scholar] [Publisher Link]

[56] Santosh K. Misra et al., "3D-Printed Multidrug-Eluting Stent from Graphene-Nanoplatelet-Doped Biodegradable Polymer Composite," *Advanced Healthcare Materials*, vol. 6, no. 11, 2017. [CrossRef] [Google Scholar] [Publisher Link]

[57] Robert van Lith et al., "3D-Printing Strong High-Resolution Antioxidant Bioresorbable Vascular Stents," *Advanced Materials Technologies*, vol. 1, no. 9, 2016. [CrossRef] [Google Scholar] [Publisher Link]

[58] Chya-Yan Liaw, and Murat Guvendiren, "Current and Emerging Applications of 3D Printing in Medicine," *Biofabrication*, vol. 9, no. 2, 2017. [CrossRef] [Google Scholar] [Publisher Link]

[59] Albert Manero et al., "Leveraging 3D Printing Capacity in Times of Crisis: Recommendations for COVID-19 Distributed Manufacturing for Medical Equipment Rapid Response," *International Journal of Environmental Research and Public Health*, vol. 17, no. 13, pp. 1-17, 2020. [CrossRef] [Google Scholar] [Publisher Link]

[60] Brian G. Beitler et al., "Interpretation of Regulatory Factors for 3D Printing At Hospitals and Medical Centers, or at the Point of Care," *3D Printing in Medicine*, vol. 8, no. 1, pp. 1-7, 2022. [CrossRef] [Google Scholar] [Publisher Link]

[61] Tjaša Kermavnar et al., "Three-Dimensional Printing of Medical Devices Used Directly to Treat Patients: A Systematic Review," *3D Printing and Additive Manufacturing*, vol. 8, no. 6, pp. 366-408, 2021. [CrossRef] [Google Scholar] [Publisher Link]